AD-A166 185 RADIATIVE AUGMENTED COMBUSTION(U) M L ENERGIA INC 1/1
PRINCETON NJ M DAVID 12 AUG 85 ENG-102-ATR-8500
AFOSR-TR-86-0085 F49620-83-C-0133

UNCLASSIFIED F/G 7/5 NL

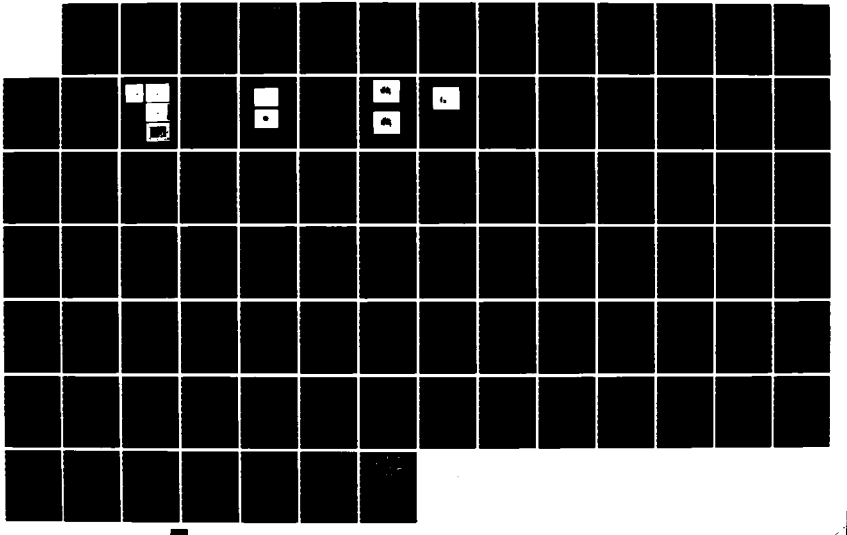

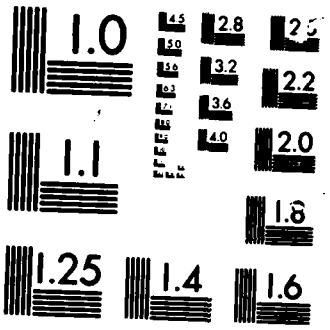

MICROCOPY RESOLUTION TEST CHART

RADIATIVE AUGMENTED COMBUSTION

MOSHE LAVID
M.L. ENERGIA, INC.
P.O. BOX 1468
PRINCETON, NEW JERSEY 08542

AUGUST 1985

SECOND ANNUAL TECHNICAL REPORT AFOSR-TR-85-
CONTRACT NUMBER F49620-83-C-0133

Approved for public release; distribution unlimited

AIR FORCE OFFICE OF SCIENTIFIC RESEARCH
BLDG. 410
BOLLING AIR FORCE BASE
WASHINGTON, D.C. 20332

"Qualified requestors may obtain additional copies from the Defense Documented Center, all others should apply to the National Technical Information Services."

Unclassified
SECURITY CLASSIFICATION OF THIS PAGE

AD-A166185

REPORT DOCUMENTATION PAGE

1a. REPORT SECURITY CLASSIFICATION: Unclassified	1b. RESTRICTIVE MARKINGS: None
2a. SECURITY CLASSIFICATION AUTHORITY	3. DISTRIBUTION/AVAILABILITY OF REPORT: Unlimited Approved for public release, distribution unlimited
2b. DECLASSIFICATION/DOWNGRADING SCHEDULE	
4. PERFORMING ORGANIZATION REPORT NUMBER(S): ENG 102 ATR 8508	5. MONITORING ORGANIZATION REPORT NUMBER(S): AFOSR-TR- 86-0085
6a. NAME OF PERFORMING ORGANIZATION: ML Energia, Inc; 6b. OFFICE SYMBOL (If applicable):	7a. NAME OF MONITORING ORGANIZATION: Air Force Office of Scientific Research
6c. ADDRESS (City, State and ZIP Code): P.O. BOX 1468, Princeton, NJ 08542	7b. ADDRESS (City, State and ZIP Code): Bolling AFB, D.C. 20332-6448
8a. NAME OF FUNDING/SPONSORING ORGANIZATION: Air Force Office of Scientific Research; 8b. OFFICE SYMBOL (If applicable): AFOSR/NA	9. PROCUREMENT INSTRUMENT IDENTIFICATION NUMBER: F49620-83-C-0133
8c. ADDRESS (City, State and ZIP Code): Bolling AFB, D.C. 20332-6448	10. SOURCE OF FUNDING NOS.

PROGRAM ELEMENT NO.	PROJECT NO.	TASK NO.	WORK UNIT NO.
61102F	2308	A2	

11. TITLE (Include Security Classification): Radiative Augmented Combustion

12. PERSONAL AUTHOR(S): Lavid, Moshe

13a. TYPE OF REPORT	13b. TIME COVERED	14. DATE OF REPORT (Yr., Mo., Day)	15. PAGE COUNT
Annual	FROM 84Jul15 TO 85Jul14	85 Aug 12	80

16. SUPPLEMENTARY NOTATION

17 COSATI CODES			18. SUBJECT TERMS (Continue on reverse if necessary and identify by block number)
FIELD	GROUP	SUB GR.	
21	01		
21	02		

19. ABSTRACT (Continue on reverse if necessary and identify by block number)

Many combustion applications are presently limited by constraints imposed by the combustion process itself, such as flammability, flame propagation, ignition and stability. Consequently much attention is being given to techniques which can augment combustion by extending these limits. One such promising technique is radiative augmented combustion. It is based on the fact that radiation of selected wavelengths is capable of photodissociating stable molecules, combustion intermediates and other inhibiting species into reactive radicals. Subsequent increases in concentrations of these radicals can modify the overall kinetics and produce radiative ignition and combustion enhancements. The potential of this technique was previously demonstrated under static conditions. Recently, it has been also demonstrated under flow conditions, with advanced vacuum ultraviolet (VUV) and ultraviolet (UV) light sources.

20. DISTRIBUTION/AVAILABILITY OF ABSTRACT	21. ABSTRACT SECURITY CLASSIFICATION
UNCLASSIFIED/UNLIMITED ☒ SAME AS RPT ☐ DTIC USERS ☐	Unclassified

22a. NAME OF RESPONSIBLE INDIVIDUAL	22b. TELEPHONE NUMBER (Include Area Code)	22c. OFFICE SYMBOL
Julian M. Tishkoff	(202) 767-4935	AFOSR/NA

DD FORM 1473, 83 APR — EDITION OF 1 JAN 73 IS OBSOLETE.

Unclassified
SECURITY CLASSIFICATION OF THIS PAGE

19. ABSTRACT (cont.)

This program emphasizes research on the interaction between VUV/UV radiation and combustion under flow conditions. The main objective is to demonstrate proof of concept by radiatively igniting combustible mixtures at conditions where thermal ignition is unreliable. Additional objectives are to provide non-intrusive (optical) flame-holding and to increase flame speed. Another important goal is to improve the fundamental understanding of the role of photochemical reactions within the whole kinetic scheme, and ultimately to identify the most effective photodissociative path. Consequently, the program is divided into two main subjects: ignition and enhancement. Each subject consists of an experimental effort supplemented by an analytical effort.

The most significant accomplishment of the experimental effort was obtaining successful radiative ignitions at very high flow velocities, up to 250 m/s. The ignition experiments proceeded to investigate the effects of equivalence ratio and Damkohler number, and a preliminary test was conducted to obtain ignition at supersonic flows. The enhancement apparatus and diagnostics have been tested and both shadow and Schlieren photographs have been obtained.

This extensive experimental effort was supported by a comprehensive analytical effort. A new model capable of simulating radiative ignition under flow conditions was developed. Its results were in good conformity with the experimental ones. They served to clarify the role of Damkohler number and to demonstrate that the VUV lamps have sufficient output to achieve ignition even under supersonic conditions.

The use of the HCT computer code to investigate radiative enhanced combustion has continued and analytical evidence for enhancement was unambigiously obtained. Dramatic increases in flame speed were achieved; 62% and 29% for photodissociation of O2 and HO2, respectively. The use of the model assisted in identifying three key factors governing radiative combustion; absorbing species, rate of radical deposition and the position of this deposition.

These results support the concept of radiative ignition and enhancement. However, the complex interactions of photochemical reactions with the overall kinetic scheme are currently not fully understood. This research will improve the understanding and will identify the most effective photodissociative paths, advancing the concept towards practical applications. This improved fundamental understanding will, in turn, assist in determining the feasibility of the concept based on the availability of newly developed light sources and their compatibility with the harsh combustion environment.

TABLE OF CONTENTS

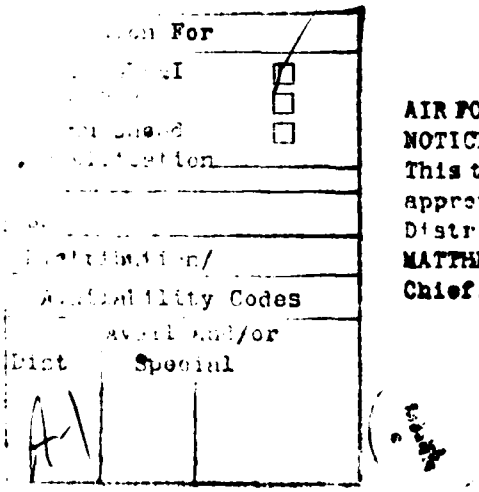

FOREWORD

This is the Second Annual Technical Report on research on Radiative Augmented Combustion conducted at M.L. ENERGIA. It is funded by the Air Force Office of Scientific Research under Contract No. F49620-83-C-0133, with Dr. J.M. Tishkoff as the Program Manager. This research succeeded and continued the work performed under a previous Contract No. F49620-81-C-0028 at Exxon Research and Engineering Co., Linden, New Jersey.

The research progress over the first year of the program, from its inception on July 15, 1983 through July 14, 1984, was reported in the First Annual Technical Report. This report describes research progress that was accomplished subsequent to that already reported. It covers the second year of the contract, from July 15, 1984 through July 14, 1985. The work was performed at ENERGIA, Princeton, New Jersey, with Dr. M. Lavid as the Principal Investigator.

ABSTRACT

Many combustion applications are presently limited by constraints imposed by the combustion process itself, such as flammability, flame propagation, ignition and stability. Consequently much attention is being given to techniques which can augment combustion by extending these limits. One such promising technique is radiative augmented combustion. It is based on the fact that radiation of selected wavelengths is capable of photodissociating stable molecules, combustion intermediates and other inhibiting species into reactive radicals. Subsequent increases in concentrations of these radicals can modify the overall kinetics and produce radiative ignition and combustion enhancements. The potential of this technique was previously demonstrated under static conditions. Recently, it has been also demonstrated under flow conditions, with advanced vacuum ultraviolet (VUV) and ultraviolet (UV) light sources.

This program emphasizes research on the interaction between VUV/UV radiation and combustion under flow conditions. The main objective is to demonstrate proof of concept by radiatively igniting combustible mixtures at conditions where thermal ignition is unreliable. Additional objectives are to provide non-intrusive (optical) flameholding and to increase flame speed. Another important goal is to improve the fundamental understanding of the role of photochemical reactions within the whole kinetic scheme, and ultimately to identify the most effective photodissociative path. Consequently, the program is divided into two main subjects: ignition and enhancement. Each subject consists of an experimental effort supplemented by an analytical effort.

The most significant accomplishment of the experimental effort was obtaining successful radiative ignitions at very high flow velocities, up to 250 m/s. The ignition experiments proceeded to investigate the effects of equivalence ratio and Damkohler number, and a preliminary test was conducted to obtain ignition at supersonic flows. The enhancement apparatus and diagnostics have been tested and both shadow and Schlieren photographs have been obtained.

This extensive experimental effort was supported by a comprehensive analytical effort. A new model capable of simulating radiative ignition under flow conditions was developed. Its results were in good conformity with the experimental ones. They served to clarify the role of Damkohler number and to demonstrate that the VUV lamps have sufficient output to achieve ignition even under supersonic conditions.

The use of the HCT computer code to investigate radiative enhanced combustion has continued and analytical evidence for enhancement was unambigiously obtained. Dramatic increases in flame speed were achieved; 62% and 29% for photodissociation of

O2 and HO2, respectively. The use of the model assisted in identifying three key factors governing radiative combustion; absorbing species, rate of radical deposition and the position of this deposition.

These results support the concept of radiative ignition and enhancement. However, the complex interactions of photochemical reactions with the overall kinetic scheme are currently not fully understood. This research will improve the understanding and will identify the most effective photodissociative paths, advancing the concept towards practical applications. This improved fundamental understanding will, in turn, assist in determining the feasibility of the concept based on the availability of newly developed light sources and their compatibility with the harsh combustion environment.

STATEMENT OF WORK

The contractor shall furnish scientific effort during the funding period, together with all related services, facilities, supplies, and materials needed to conduct the following research. The professional manpower level of this Work Statement is 1,550 man-hours.

a. Provide a combustion test facility capable of conducting radiative ignition and enhancement experiments under flow conditions.

b. Select and employ the most appropriate VUV/UV sources from currently available devices.

c. Design and conduct radiative ignition tests under flow conditions; investigate effects of equivalence ratio, pressure and velocity (mostly laminar) on radiative ignition; measure radiative ignition energies under flow conditions; and compare them with conventional spark ignition data.

d. Conduct radiative enhancement experiments under flow conditions, measuring enhancement in terms of changes in the fundamental burning velocity and developing highly sensitive measurement techniques to sense changes in the burning velocity.

e. Incorporate into the static initiation (ignition) model the convection heat and mass (species) transfer terms. Compare experimental data with model predictions. Undertake additional model revision and refinement as deemed necessary from the comparison.

f. Modify and revise the HCT model to simulate radiative enhancement under static and flow conditions. Calculate flame propagation properties and compare with experimental data. Use the model to explore the interaction between spectral absorptance and subsequent photo and chemical kinetics, and transport phenomena in reacting flow systems.

g. Perform calculations to find the optimum conditions for deposition of radiative energy in the reaction zone and to determine the radical production that results from this radiation. Include the effects of wavelength-dependent optical properties, such as absorption coefficients, transmittance, and also temperature sensitive reaction rates.

STATUS OF THE RESEARCH

The period of performance of the entire Radiative Augmented Combustion program is thirty-six months (1), and the present contract awards cover the first twenty-four months (2). The research progress over the first twelve months, from the inception of the program on July 15, 1983 through July 14, 1984, was reported in the First Annual Technical Report (3). This section reports on recent research progress that was accomplished subsequent to that already reported. It covers the period of performance of the second contract year, from July 15, 1984 through July 14, 1985. It is divided into two main efforts; Experimental and Analytical. Each effort consists of two research topics; radiative ignition and radiative combustion enhancement.

A. EXPERIMENTAL EFFORT

In the previous proposal (1, 2) experiments were proposed to investigate photochemical ignition under flow conditions and photochemical enhancement of burning velocities. Both of these objectives were significantly advanced during the last contract period. A flow reactor for the study of photochemical ignition was designed, built, and extensive experimentation was accomplished. A pancake burner to study photochemical enhancement of premixed gaseous flames was built and tested along with its associated optical diagnostic equipment. This system has been operated with propane/air and hydrogen/air flames both with and without ultraviolet irradiation from the EIMAC lamp.

The ignition and enhancement experiments are discussed separately in the following sections.

1. Experimental Work on Radiative Ignition

After several design studies, the flow reactor design that was previously proposed for this work (2) was replaced in favor of a simpler and analytically more tractable design. It is shown in Figure 1.

The test section was made from a section of 1/2 inch O.D. stainless steel tubing approximately 20 inches long. Halfway along the length of the tube a slot was milled into it of such shape as to hold a cylindrical ILC lamp with the outer face of its window near the centerline of the tube. This design eliminated the use of LiF windows between the VUV source and the mixture, thus eliminating one set of window losses. Hydrogen and oxygen were admitted to the upstream end of the tube through

separate legs of a "Tee". They mixed at the "tee" and as they flowed along several feet of tubing (at least 4 ft of 1/4 in. O.D. tubing or at least 10 ft of 1/2 in. O.D. tubing, depending on the flow rate) to the inlet of the test section. The position of the lamp is over 20 tube diameters downstream from the inlet end of the tube to assure fully developed flow at that position. The lamp was sealed in the tube with silicone rubber.

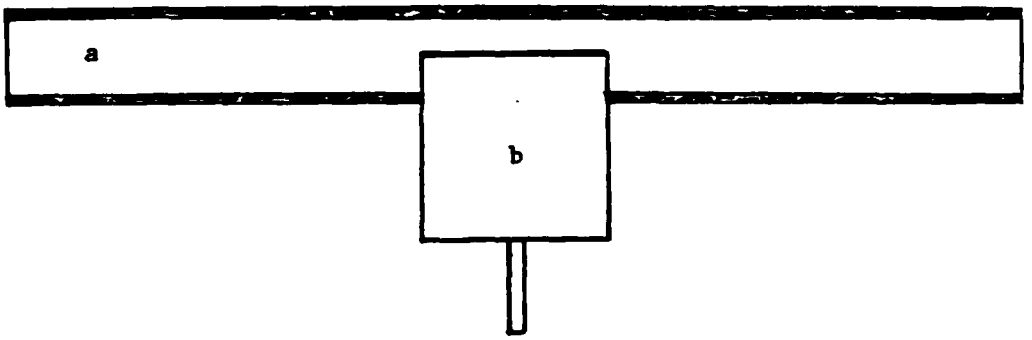

Figure 1.

Radiative Ignition Apparatus For Flow Condtions
a. Flow reactor, b. ILC Lamp

The system required rather substantial flows of hydrogen and oxygen, (3.6 liters/s to produce a Damkohler number of unity) much of which was exhusted from the test section unburned. Experiments with low flowrates (high Damkohler numbers) were performed in a standard chemical hood, and experiments with high flowrates (low Damkohler numbers) were performed outside on a field adjacent to the laboratory.

Ignition experiments were conducted in the following manner. Hydrogen and air flow rates were set to give the desired equivalence ratio and flow velocity within the test section. The lamp power supply was set to give the required number of joules per pulse, and the pulse rate was set at 3.2 pulses per second. Then, the experiment was run for as many as forty pulses. Ignition was detected by an audible "pop" from the apparatus (at low Damkohler numbers this "pop" became a sharp window rattling "crack"). If no ignition was obtained, the pulse energy was set at a higher value and the experiment was repeated. When ignition was obtained, the experiment was repeated at gradually reduced pulse energies (the least energy increment was 1/2 joule) until ignition was no longer obtained (after obtaining ignition the system would usually ignite at lower energies than was the case prior to the first ignition). The least energy at which ignition was obtained during this decreasing energy progression was taken as the minimum ignition energy.

The definition of the Damkohler number is that it is the ratio of convective time to chemical reaction time. For our work this was taken as the ratio of the time for a flow element to pass over the apature of the lamp window (0.75 cm) to the radiative pulse width (approximately 0.0001 s).

The results from this work are presented in Figure 2. This figure gives the minimum ignition energy in joules per pulse that was delivered to the lamp from the power supply as a function of Damkohler number for several equivalence ratios. It is important to note that the pulse repetition rate was sufficiently high that the power supply capacitors did not have time to fully charge between pulses. Therefore, the energy delivered was less than the energy set (stored) on the capacitors in the power supply. This fact was corrected as described below.

The ratio of delivered voltage to set voltage for a fixed repetition rate is a function of how the capacitors are connected in the power supply. The two capacitors were connected in series for energy ranges from 0 to 12.5 j, one capicitor only for energy ranges from 0 to 25 j, and in parallel for ranges from 0 to 50 j. For the 0 to 12.5 j range, the ratio of delivered to set voltage was measured to be 0.867, and for the 0 to 50 j range it was 0.688. Measurements for the 0 to 25 j range were not conducted and the ratio for this intermediate range was taken as an average of the high and low ranges (i.e. 0.778). This intermediate range affected only two points. The ratio of the energy delivered to energy set is the square of these voltage ratios. Consequently, the set ignition energy was corrected for this effect to give the true electrical energy delivered to the lamp, and it is this energy that was plotted in Figure 2.

Examining the results shown in Figure 2, it is revealed that minimum ignition energy is least for 0.5 equivelence ratio and increases for either fuel-leaner (0.3), or fuel-richer mixtures (0.7 and higher equivalence ratios for which it is about the same). This new experimental finding that fuel-lean mixtures are more favorable for photochemical ignition, is an important corroboration to previous results obtained with excimer lasers under static conditions (4). The experimental results also indicate that minimum radiative ignition energy is relatively independent of Damkohler number for numbers greater that one, but it is a strong inverse function of Damkohler numbers less than one.

This radiative ignition system was analytically modeled, and initial results were reported in referance (5). However, the original model did not include oxygen atom recombination reactions. It has since been expanded to include that effect. The derivation of the model with O-atoms recombination is given in Appendix A, and the results are included in the section on Analytical Effort.

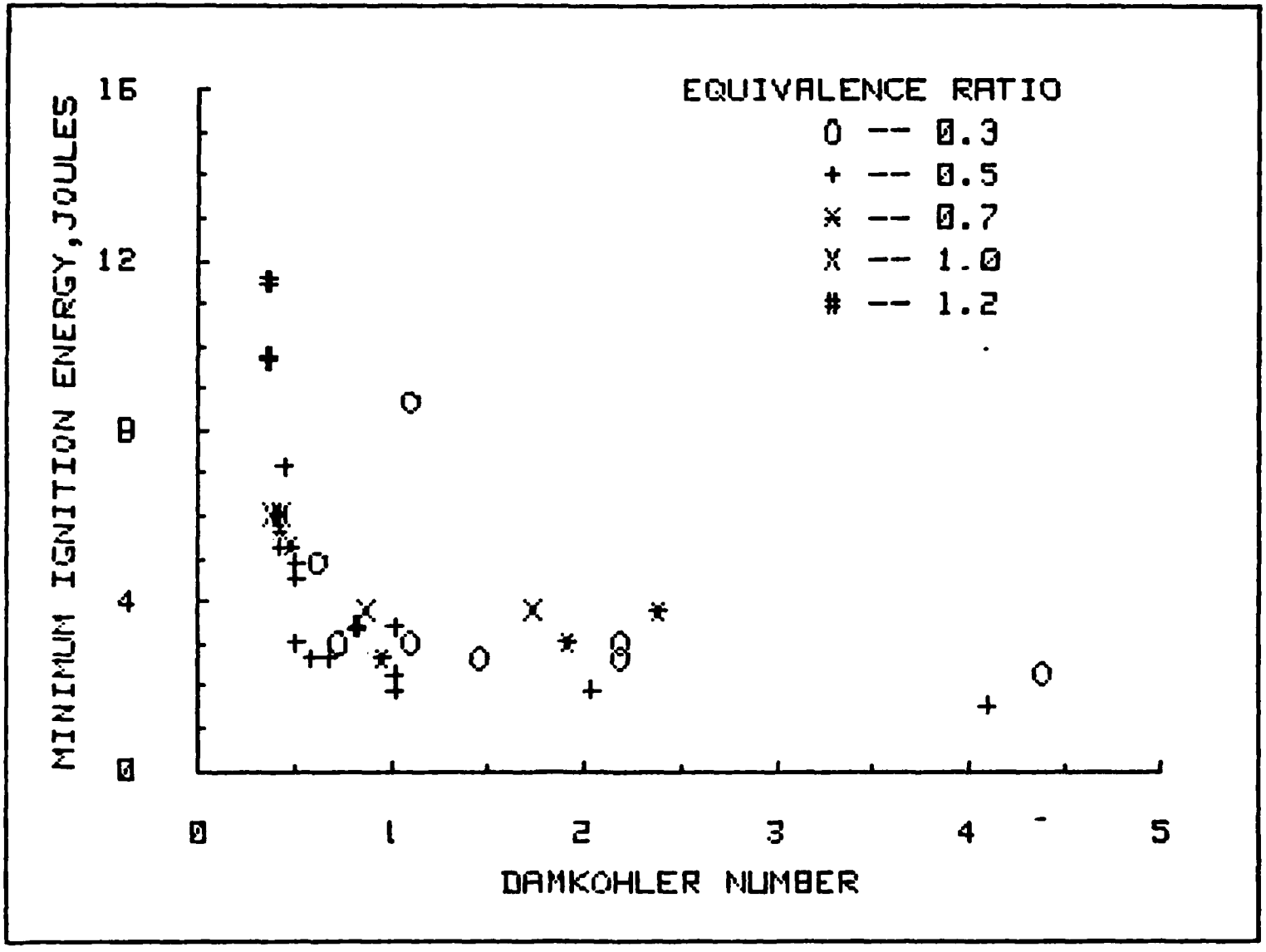

FIGURE 2.

RADIATIVE MINIMUM IGNITION ENERGY VS. DAMKOHLER NUMBER
FOR HYDROGEN-AIR MIXTURES AT VARIOUS EQUIVALENCE RATIOS

These recently obtained experimental results demonstrate that photochemical ignition is feasible for high speed gas streams even at relatively low pulse energies, (we got ignition with as little as three joules), provided the pulse duration is sufficiently short. Flows at still higher velocities may be ignited with low radiative energies if the pulse width is further shortened. This is true because Damkohler number is inversely proportional to the product of pulse width and flow velocity. Thus, raising one while lowering the other to keep their product constant, can maintain constant Damkohler number. By properly controlling pulse width (and thus Damkoler number) this technology may be used to ignite even hypersonic flows.

The idea of using VUV irradiation for supersonic flows, which are known to be very difficult to ignite, was tested at NASA Langley Research Center. A very preliminary and limited test was conducted using the Mach 2 nozzle described in reference 6. The same ILC light sources, used in the experiments described above, were installed on the supersonic combustor as shown in Figure 3. The combustible mixture was hydrogen-air at a low stagnation temperature of about 1800 R and at equivalence ratios of 0.4 to 1.0.

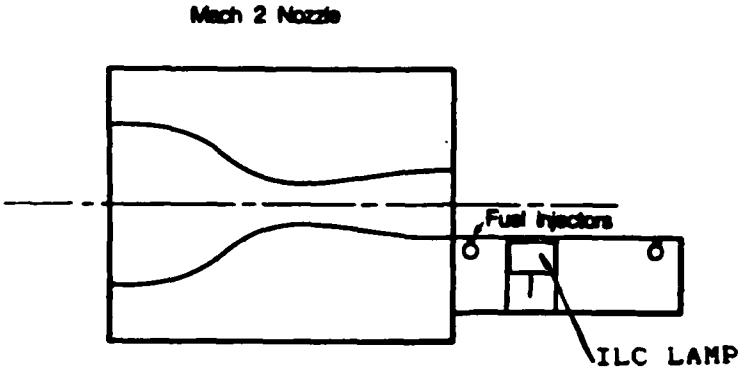

Figure 3.

Schematic of Mach 2 Apparatus

In the first series of runs (Runs #35) the lamp was installed at the bottom of the test section irradiating upward. Strong and intensive kernels were observed on the UV TV monitor, but full combustion was not obtained (Figure 4, a & b). However, as the flow became subsonic, yet at very high velocity (250 m/s), ignition was detected (Figure 4, c).

d M<1

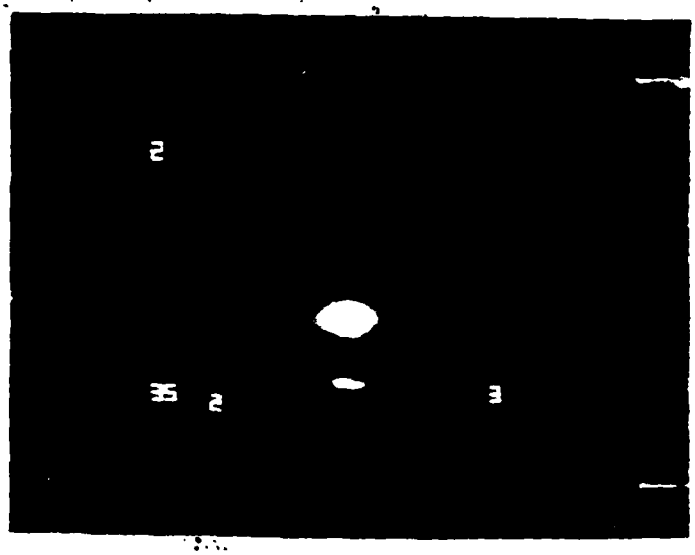

a

M = 2

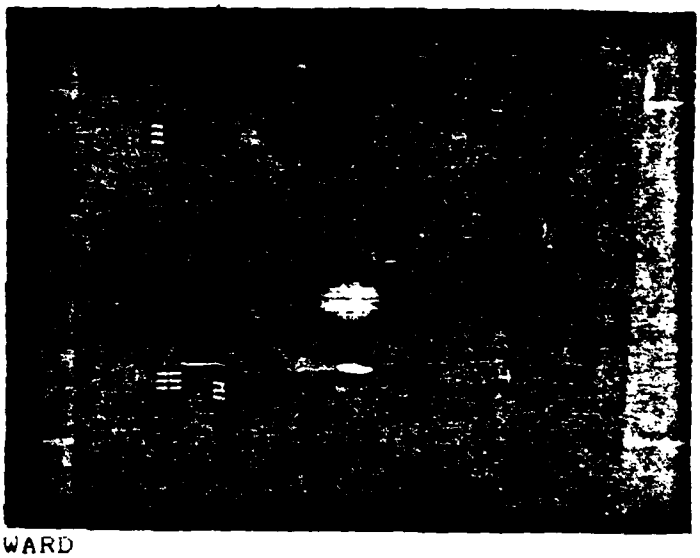

b

M = 2

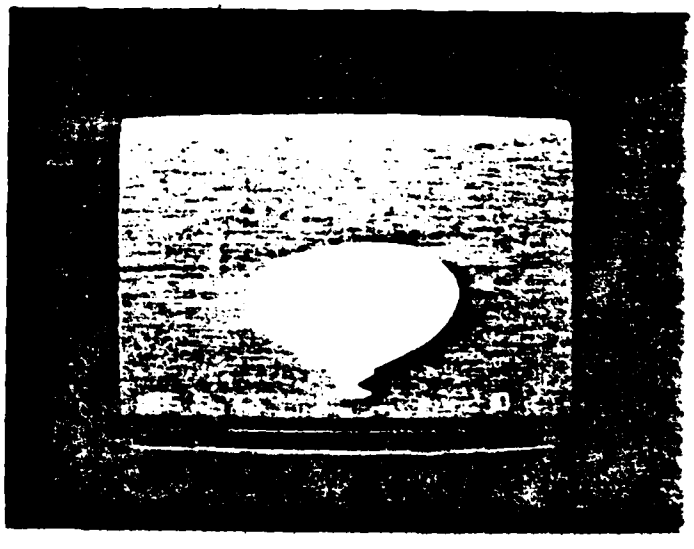

c

M < 1

FIGURE 4.

RUNS #35
H2/AIR, ILC LAMP IRRADIATING UPWARD
WITHOUT WEDGE

In the second series of runs (Run #36), the lamp was installed at the top of the test section irradiating downward. In addition, a wedge was inserted upstream of the lamp to improve mixing. similar results were obtained, partial ignition at supersonic conditon and full ignition at subsonic conditon as shown in Figure 5, a & b, respectively.

We concluded that the lack of sustained combustion at supersonic flows was due to either inadequate mixing at the vicinity of the lamp (as can be seen in Figure 4, a, from the relative large distance, 1/4", between the lamp's window and the ignition kernel, indicating low concentration of O2 at the window), and/or insufficient light intensity for such high velocity (Da = 0.1). Before further attempts are made, a solution to these two problems will be sought.

The successful subsonic ignitions extend the scope of our experiments by allowing us to reach higher velocities. Moreover, based on NASA's results we incline to believe that there is *no* conceptual difference between subsonic and supersonic photochemical ignitions, provided equal quantities of radiation are absorbed by the fluid element at the ignition kernel under both conditions. This point can be substantiated by comparing the ignition kernels in supersonic flow (Figure 4, a) and in subsonic flow (Figure 4, d). Under both conditions the kernels are very similar.

Another point worth examining is the adequacy of light intensity. This can be achieved by conducting two different photochemical ignition experiments. In the first experiment, the supersonic velocity be decreased from M = 2 to about M = 1.5. In other words, Damkohler number will be increased to favor ignition, yet supersonic flow is still maintained. In the second experiment, the stagation temperature can be increased until photochemical ignition is obtained. This provides a combination of thermal and photochemical dissociation, thus, lowering the light intensity required to obtain ignition as compared to photochemical ignition alone.

Lastly, as previously discussed, combustible mixtures at supersonic and even hypersonic conditions may be photochemically ignitable by properly controlling the pulse width of the VUV light source. To prove this point, preparations are being made to use the newely obtained VUV CERMAX lamps in a pulsed mode. These lamps have much more VUV output than the ILC lamps, however they are designed for a continuous mode operation. We are in the midst of modifying the electrical circuit to provide a pulsed mode. After the modification is completed these CERMAX lamps will be first tried under subsonic conditions, and if successful, will be used on the Mach 2 nozzle of NASA Largley.

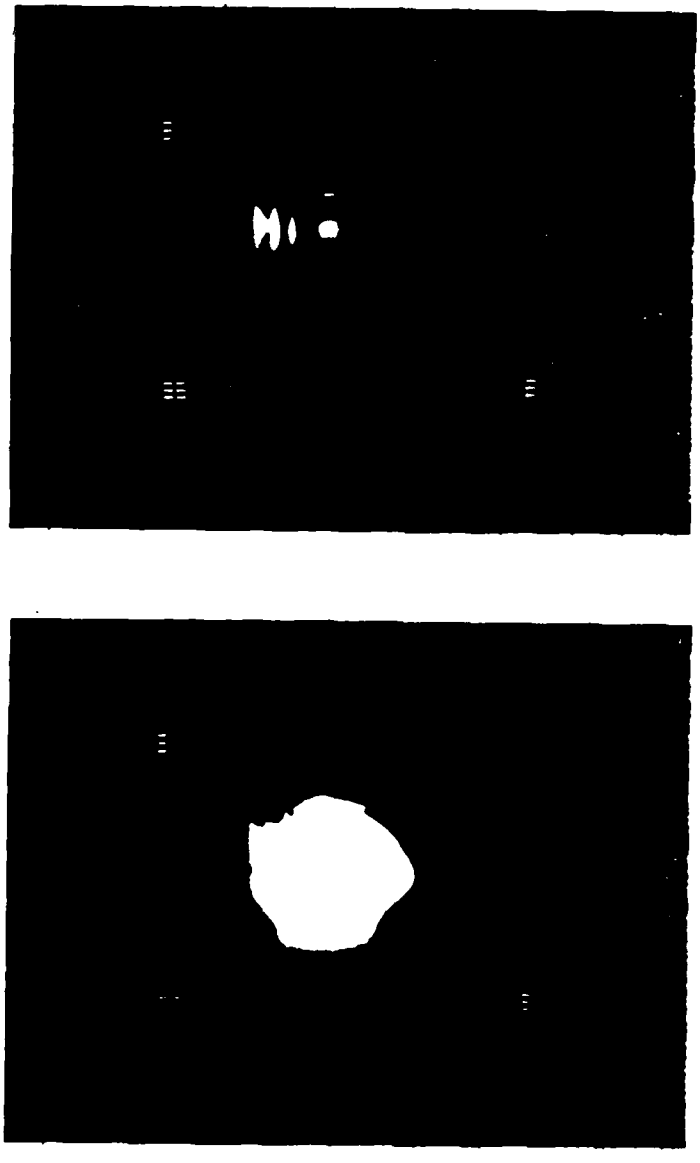

a

M = 2

b

M 1

FIGURE 5.

RUNS #36
H2/AIR, ILC LAMP IRRADIATING DOWNWARD,
WITH WEDGE

2. Experimental Work on Radiatively Enhanced Combustion

The pancake burner that was described in reference 3 has been designed, built, and put into operation. The combustible mixture exits as a jet from a small orifice in the thin top plate of a plenum chamber producing a conical flame. The orifice diameter is of the order of two mm and the optical pathlength from the window to the flame front is very short, 2-4 mm. This "pancake" design was chosen because of the experimental simplifications it offers in achieving axisymmetric illumination with short optical pathlengths. It also has the window on the cold reactants side of the flame where it is not subjected to the high temperature of the products. It has been operated with propane/air and hydrogen/air flames, both illuminated and non-illuminated. Initial problems were encountered with the configuration of the flame and with the accurate determination of its shape and size. These problems have been addressed through adjustments of the burner port size and through improvemetns in the diagnostics.

The diagnostic system for measuring changes in flame cone angle to determine changes in burning velocity was discussed in reference 3 Appendix B. It has been designed, built and tested. Both shadow and schlieren photography have been used. While the shadow technique has been the most successful technique used thus far, the optical system is being refined to fully exploit the inherent advantages of the schlieren technique (3). The diagnostic light source is a He:Ne laser with output in the visible red. The output beam is diverged with a negative lens, intercepted with a 6 inch diameter, 60 inch focal length front surface spherical mirror (the collimating mirror), passed to a similar mirror (the focussing mirror) thence over the test section, through the focal point (at the knife edge in the case of a schlieren), and onto a projection screen. Direct photography was not used because of inadequate luminosity emitted by hydrogen-air flames in the visible spectrum.

Figure 6 is a shadowgraph of a hydrogen-air flame without ultraviolet illumination. The right-hand two thirds of the burner plate is shown in profile with the flame located at its center. The flame is clearly visible as dark cone surrounded by a jet of burned gas. The outer edge of the dark zone is the flame front.

Figure 7 shows a similar shadowgraph with the VUV light on and shining up through the gas port in the plate. This demonstrates that the intense VUV output has no adverse effect on the clarity of the image.

Figure 6.

Shadowgraph of Hydrogen-Air Flame Without VUV Illumination

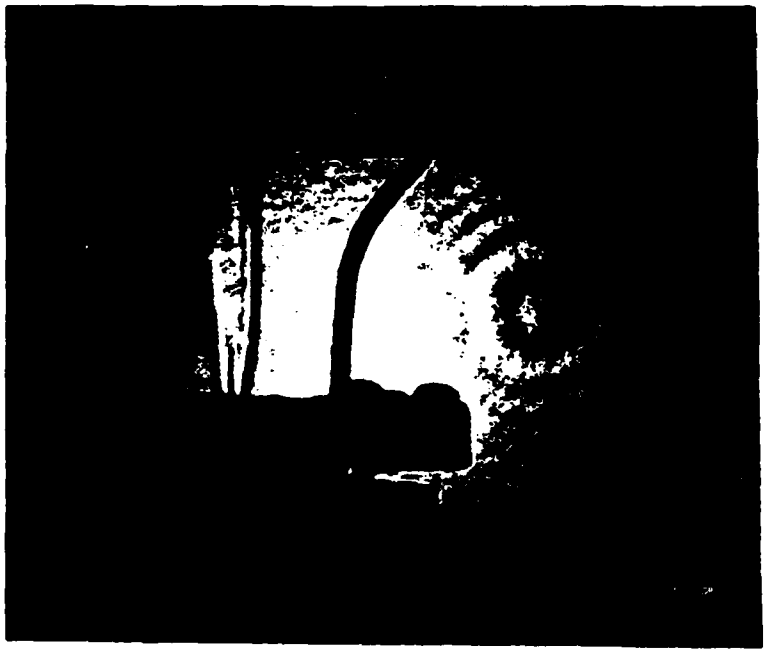

Figure 7.

Shadowgraph of Hydrogen-Air Flame With VUV Illumination

Figure 8 is a schlieren photograph of the unilluminated flame. In this figure the flame cone is rendered as a bright central zone.

Figure 8.

Schlieren Photograph of Hydrogen-Air Flame Without VUV Illumination

These figures were taken during shakedown of the apparatus and they were not intended to produce quantitative data. However, they provide valuable information about the flame half angles, which are approximately 4 degrees. The sensitivity of the half angle, θ, to relative change in burning velocity Uo is given by:

$$d\theta = \tan \theta \, dUo/Uo$$

Thus, to detect a 10 percent change in burning velocity around θ = 4 degrees (at constant gas jet velocity U), it is necessary to resolve an angular change of 0.4 degrees. This is quite achievable as our initial results demonstrate, but our control and imaging techniques must be improved.

To make detection easier, it is desirable to stabilize the flame at lower jet velocities, U, resulting in shallower flames with larger cone half angles. For example, if a half angle of 10 degrees can be achieved with a stable flame, then a 10 percent change in burning velocity will result in a one degree change in

half angle, and a corresponding decrease in the value of the minimum detectable burning velocity change. Such improvements in flame geometry will be an important part of our forthcoming efforts.

In addition, the jet velocity U must be held rigorously constant both with and without illumination or corrections must be made for the effects of jet velocity variation. These corrections have been derived.

The system was found exceedingly sensitive and capable of responding even to very small changes of density generated by the hydrogen-air flames near the fuel-lean flammability limit. The experimental technique will be further refined during the next contract period to produce the anticipated enhancement in flame speed.

STATUS

In summary, during the last contract period the experimental effort has:

- o Designed and fabricated apparatus for testing radiative ignition under flow conditions.
- o Investigated photochemical ignition of H2-air mixtures over the equivalence ratio range 0.3 to 1.2 for Damkohler numbers in the range 0.36 to 4.4 (a velocity range from 208 to 17 m/s, respectively).
- o Conducted preliminary radiative ignition tests at supersonic conditions (M=2).
- o Obtained successful radiative ignition at high flow velocities, up to 250 m/s.
- o Concluded that combustible mixtures at supersonic (and even hypersonic) conditions may be photo-ignitable by properly controlling the VUV power.
- o Designed and fabricated a pancake burner for studies of radiative burning velocity enhancement.
- o Installed the EIMAC light source on the burner and tested it with both propane/air and hydrogen/air flames.
- o Developed shadow and schlieren diagnostics for detecting enhancement in burning velocity.

B. ANALYTICAL EFFORT

The experimental effort described above was complemented by an analytical effort which also proceeded on two fronts: ignition and enhancement.

1. Radiative Ignition in Flow Systems

To gain essential insight into the experimental work on radiative ignition in flow systems, it became necessary to investigate the problem theoretically. Accordingly, a generalized theory of the problem was constructed and then particularized to the experimental configuration. The details of the theorectical development are contained in Appendix A. In brief, the model considers the photodissociation reaction O2 + hv ---> 2O, which is excited by a 0.0001 s , square pulse of input radiation, and the opposing three body recombination reaction O + O + M ---> O2 + M.

The criterion for ignition is that it occurs when the photochemically induced oxygen atom number density achieves a value of 1E16 atoms/cc. This value represents 0.06% dissociation, for stoichiometric hydrogen/oxygen at atmospheric pressure and 298 K, since at these conditions the molecular oxygen number density is 8.2E18 molecules/cc. This is the order of magnitude of the critical oxygen atom number density that was also calculated in reference 3 for static systems. The dependent variable is the criticality ratio, F, which is defined as the ratio of oxygen atom density to the critical oxygen atom density. Thus, when F is equal to or greater than unity, ignition occurs.

The general theory was particularized to a two-dimensional model of the experimental system. A schematic diagram of the model is shown in Figure 9.

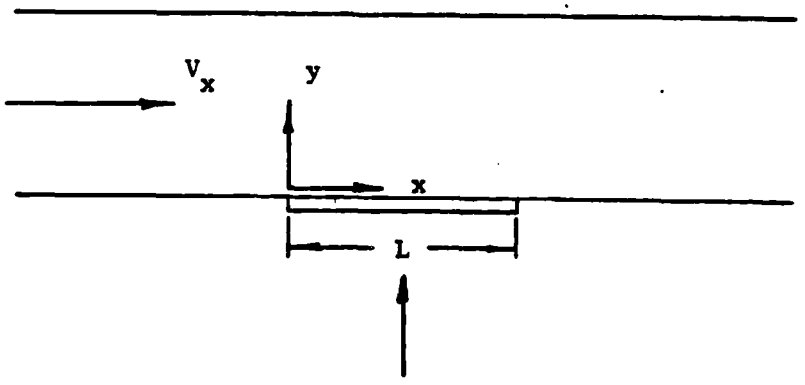

Figure 9

Schematic Diagram of the Photochemical Ignition Model

In the model, x is measured along the flow direction from the leading edge of the window, which is the origin of coordinates. All space dimensions are non-dimensionalized by the window diameter L, and time is non-dimensionalized through the pulse width ti. The Damkohler number, D, was defined as the ratio of the convective time across the window (i.e. through the beam of parallel light from the pulsed lamp) to the radiation pulse width (i.e. the photochemical reaction time).

Several important assumptions were made in setting up this model. They are:

1. Diffusion is negligible over the duration of the radiative pulse.

2. Only two chemical reations (photodissociation opposed by recombination) are considered important over the duration the pulse.

3. Flow velocity, Vx, is constant throughout the field.

4. The spectral absorption coefficient, while wavelength dependent, is constant throughout the field for any given wavelength.

Assumption 1 is undoubtedly very good on the 1E-4. scale of the radiative input pulse, although it might have to be relaxed if one chooses to study quenching phenomena within microns or less from the surface of the window. Assumption 2 is reasonable. The first reaction, O2 + hv ---> 2O, simulates the photochemical effect. The second reaction is the opposing three body recombination (i.e. O + O + M ---> O2 + M). The rate constant for this reaction was taken as 3.59E15 cm6/mole2 sec. This recombination reaction was included because it represents a major loss to the system. Other chain reactions that are involved in the ignition process were already incorparated in deriving the critical number density. Assumption 3 is non-essential. Any flow field can be readily imposed on the system. However, a uniform flow field simplifies the interpretation of the results, and results from this case can be extrapolated to other flow fields so long as assumption 4 is reasonable. Assumption 4 depends for its validity upon the degree of photochemical dissociation that is achieved. If the O2 concentration is constant throughout the field, then so is the spectral absorption coefficient, and assumption 4 is exact. For small percents dissociation assumption 4 is excellent. However, when F reaches 100 for stoichiometric hydrogen/oxygen at standard conditions, approximately 6 percent of the O2 is dissociated and asaumption 4 begins to degenerate. When F reaches approximately 800, all of the O2 is dissociated and assumption 4 is void. In our work the important criterion is satisfied when the system achieves the critical number density. At that point only 0.06 percent of the O2 is dissociated and assumption 4 is excellent.

The spectral characteristic of the radiation source is that of the ILC lamp as shown in Figure 10 (1).

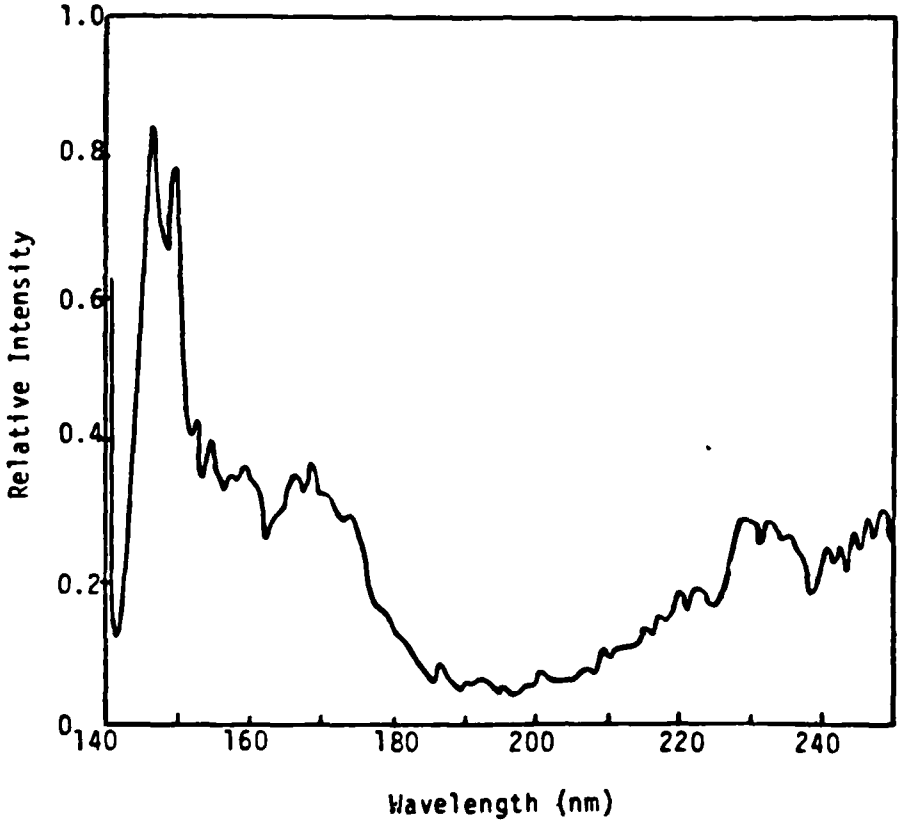

Figure 10.

Spectral Distribution of Intensity of the ILC Lamp.

The spectral absorptivity for O2 (at standard conditions) is shown in Figure 11 which is constructed from the data of reference 7. Notably, the ILC lamp is rich in energy at the short wavelengths, where the spectral absorptivity is the greatest. Over the wavelength range of the lamp (145 to 245 nm) the spectral absorptivity falls sharply from 3.96E2 to 1.35E-5 per cm. Thus, the deposition of photons within the gas is extremely wavelength dependent.

The model was evaluated for the following input conditions:

Stoichiometric hydrogen/oxygen

P = 1 atmosphere

T = 298 K

Electrical energy input to lamp = 3 joule

Lamp efficiency in VUV = 2 percent of electrical input

Lamp output in VUV = 0.06 joule

Window (beam) diameter = .75 cm

Pulse width = 0.0001 s

Critical number density for ignition = 1E16 atoms/cc

Damkohler number range = 0.001 to 10

Velocity range = 7.5E6 to 750 cm/sec

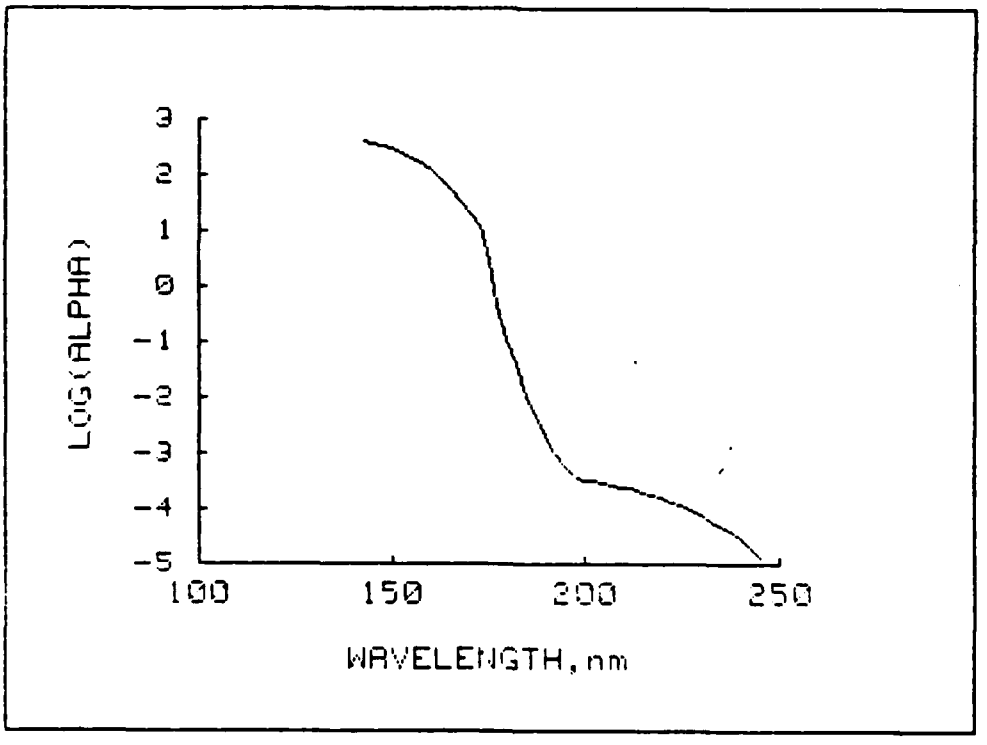

Figure 11.

Spectral Absorption Coefficient (1/cm) for Molecular Oxygen at Standout Conditions, (plotted from date of reference 7).

The results of this work are shown in figures 12 through 20. Figures 12-15 show the criticality ratio (the ratio of local O-atom number density to the critical value for ignition) as a function of axial distance along the stream at the adjacent surface to the input window (i.e. at zero depth in the stream). In these figures the window extends from 0 to 1.0 (dimensionless) along the abscissa. All these figures refer to 0.06 j of light output from the ILC lamp distributed over a spectral range from 145 to 245 nm as shown earlier in Figure 10, (except in the case of Figure 16). The 0.06 j output represents our lowest experimental ignition energy of 3 j at a 2 percent lamp efficiency in the VUV region. They all show the effect of Damkohler number, and taken in sequence they clearly demonstrate the effect of window transmittance or optic contamination. Figure 12 has no filter (contamination) but the other three figures (13,14,15) have longpass filters with various short wavelength cutoffs at 155, 165 and 175 mn, respectively. The effect of short cutoff (hard ultraviolet loss) is profound (note the scale change for Figure 15). This profound effect of short cutoff reflects the dramatic decrease of O2 absorptivity with increasing wavelength (see also Figure 11).

In order to examine the effect of wavelength dependence on the criticality raitio we focus our attention on constant Damkohler number (i.e. D=1). In the case of spectral distribution from 145 to 245 nm without a filter the criticality ratio reaches a value of 36 near the leading edge of the window. When a filter is installed and the radiation between 145 and 155 is cutoff (only 10 nm from a range of 100 nm), this ratio is significantly decreased to a value of 12 (Fig. 13). In Figure 14 the VUV radiation between 145 and 165 nm is eliminated from the lamp (additional increment of 10 nm) and the ratio falls to 8. Moreover, this value is reached further downstream from the leading edge. From these runs we conclude that it is only the shortwavelengths that interact strongly with molecular oxygen. Figure 16 emphasizes this point. It is the case where the entire 0.06 j is irradiated at 175 to 245 nm range, and there is no filter loss of total energy as in the previous filtered cases. Figure 15 represents the same spectral distribution (175 to 245 nm) exept that it has a filter that cuts off energy between 145 to 175 nm, causing a reduction of about 30% in the 0.06 j output as compared to Figure 16. Comparison between the results for D = 1 reveals that the criticality ratio is only slightly decreased from 0.6 (Fig. 16) to 0.5 (Fig. 15). Both values are obtained at the trailing edge of the window. This finding shows that the reduction in criticality ratio stems almost entirely from loss of absorption, and not from decrease of radiative energy.

The effect of Damkohler number on radiative ignition can be studied by examining the results represented by any of the figures 12 through 16.

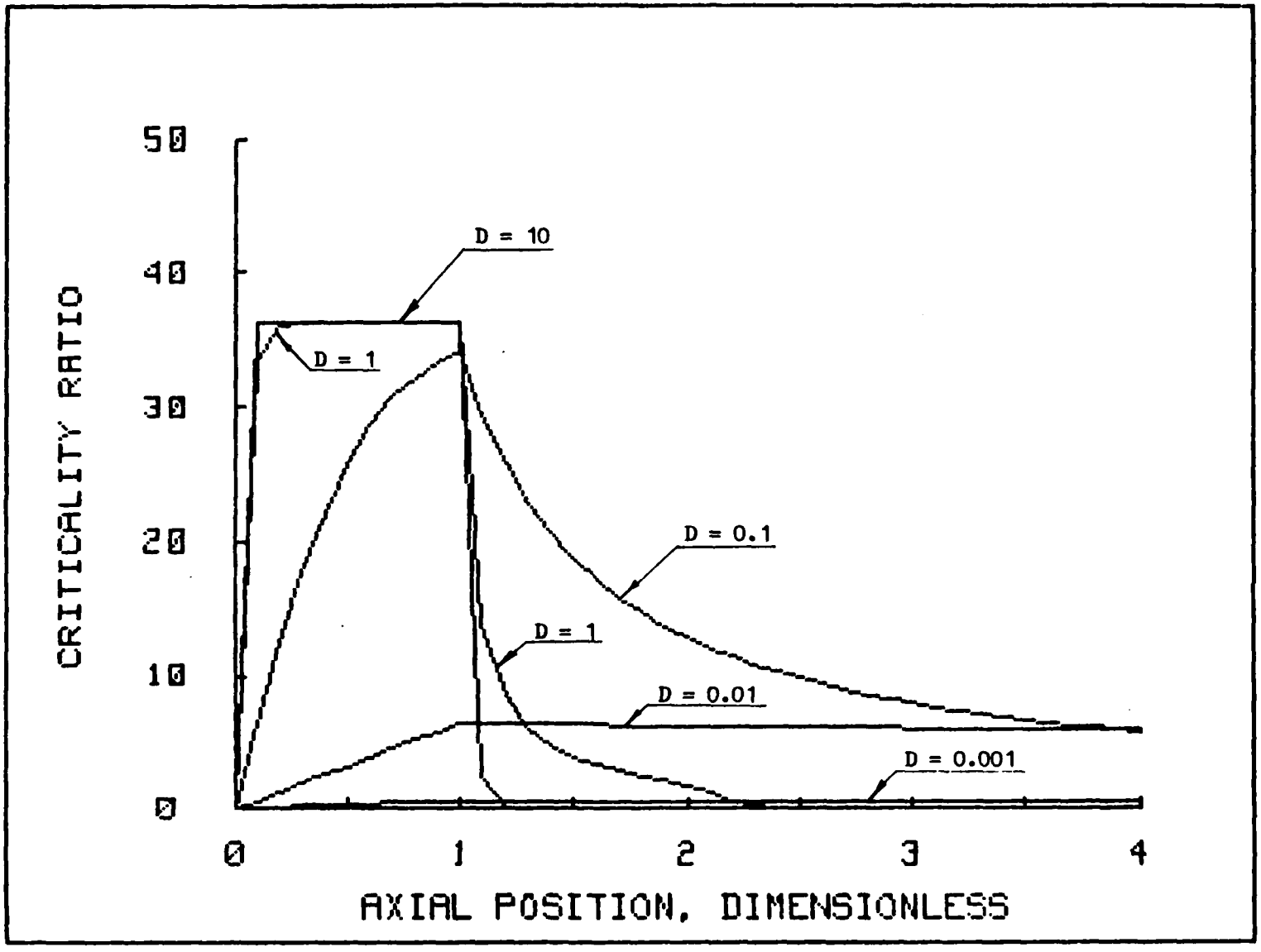

FIGURE 12.

CRITICALITY RATIO AT WINDOW ALONG ITS AXIS FOR VARIOUS DAMKOHLER NUMBERS, EQUIVALENCE RATIO 1.0, RADIATION ENERGY INPUT 0.06 j IN SPECTRAL RANGE 145 to 245 nm, NO FILTER

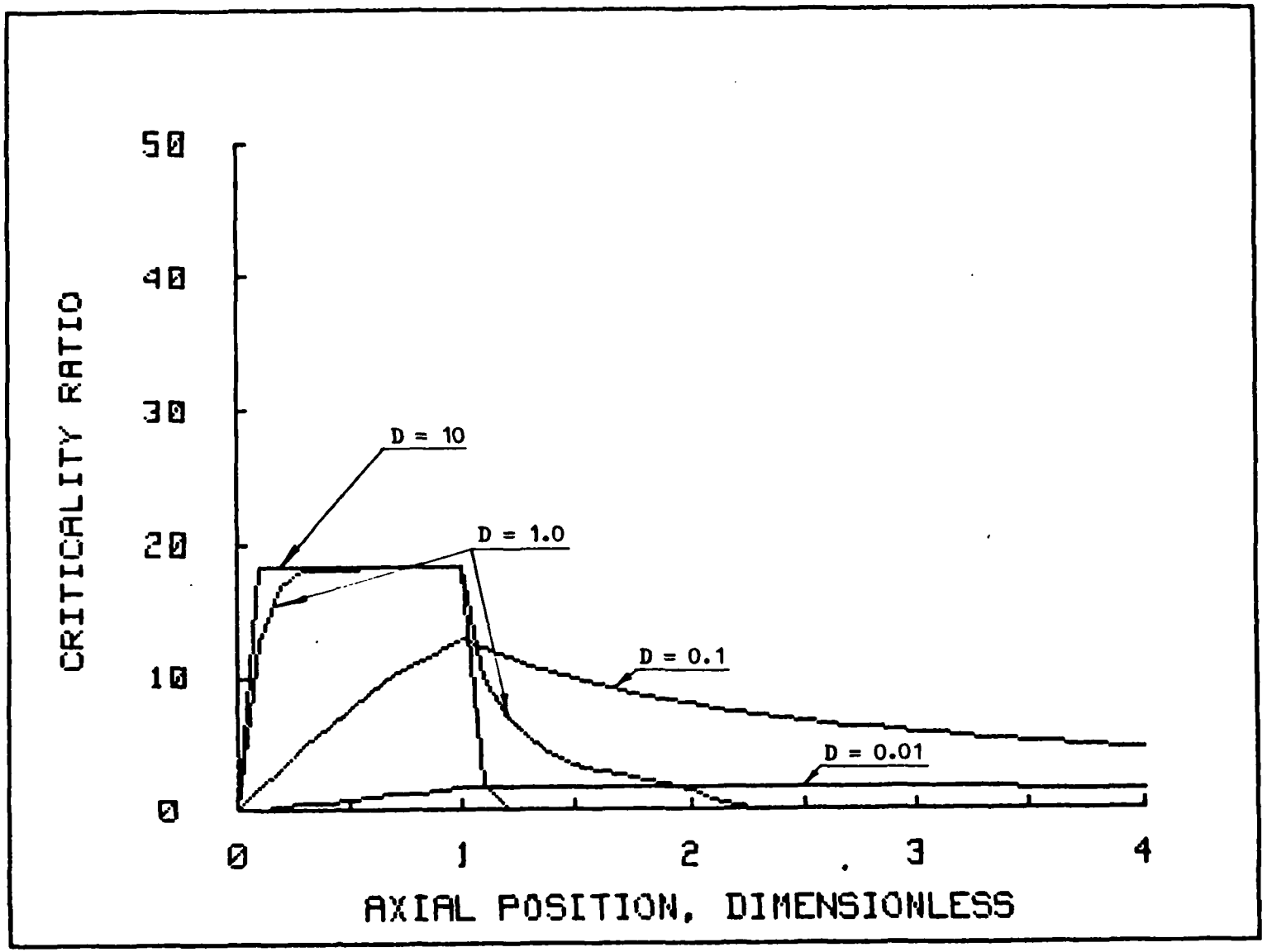

FIGURE 13.

CRITICALITY RATIO AT WINDOW ALONG ITS AXIS FOR VARIOUS DAMKOHLER NUMBERS, EQUIVALENCE RATIO 1.0, RADIATION ENERGY INPUT 0.06 j IN SPECTRAL RANGE 145 TO 245 nm, FILTER: 155 nm LONGPASS CUTOFF

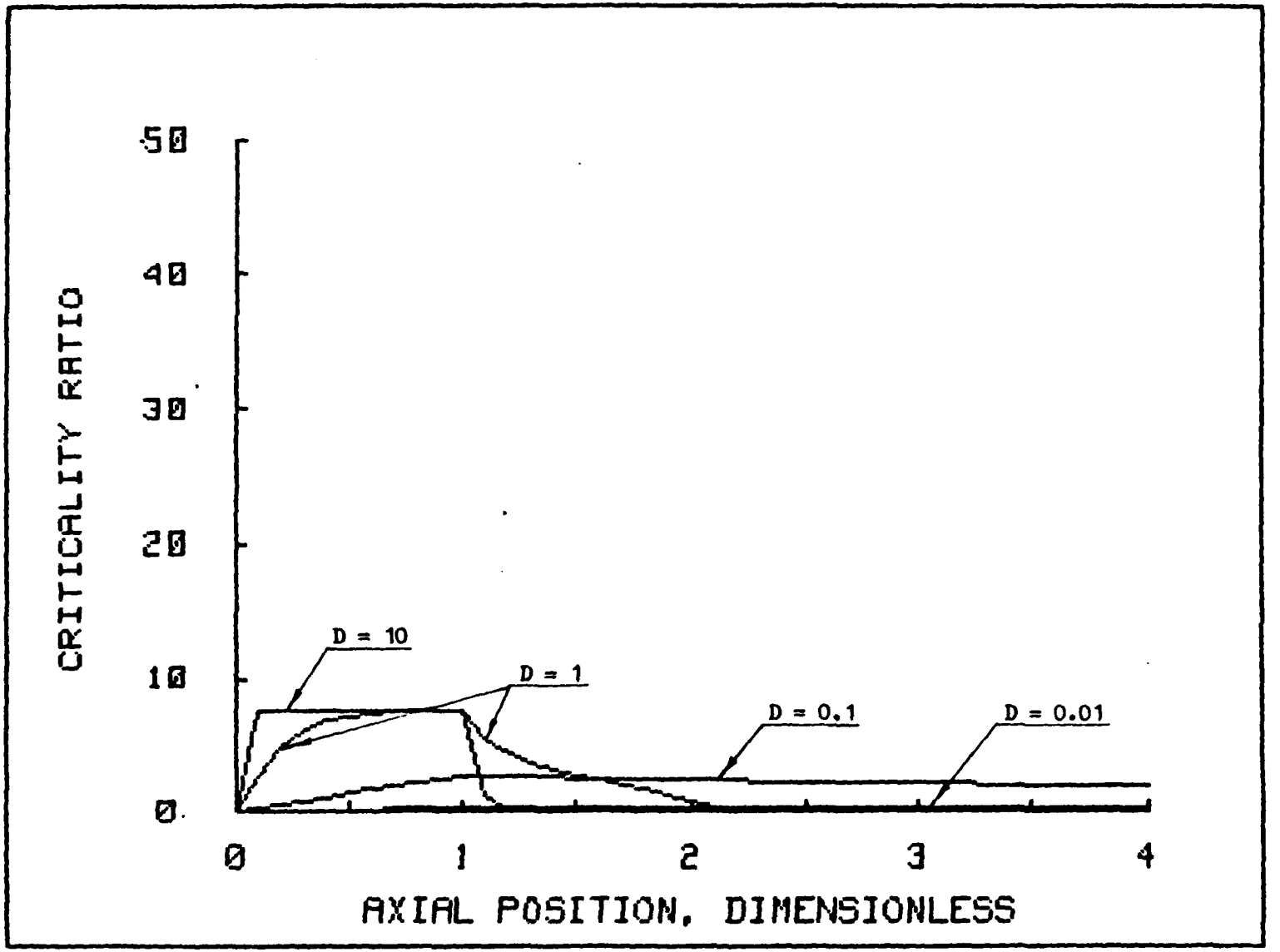

FIGURE 14.

CRITICALITY RATIO AT WINDOW ALONG ITS AXIS FOR VARIOUS DAMKOHLER NUMBERS, EQUIVALENCE RATIO 1.0, RADIATION ENERGY INPUT 0.06 j IN SPECTRAL RANGE 145 TO 245 nm, FILTER: 165 nm LONGPASS CUTOFF

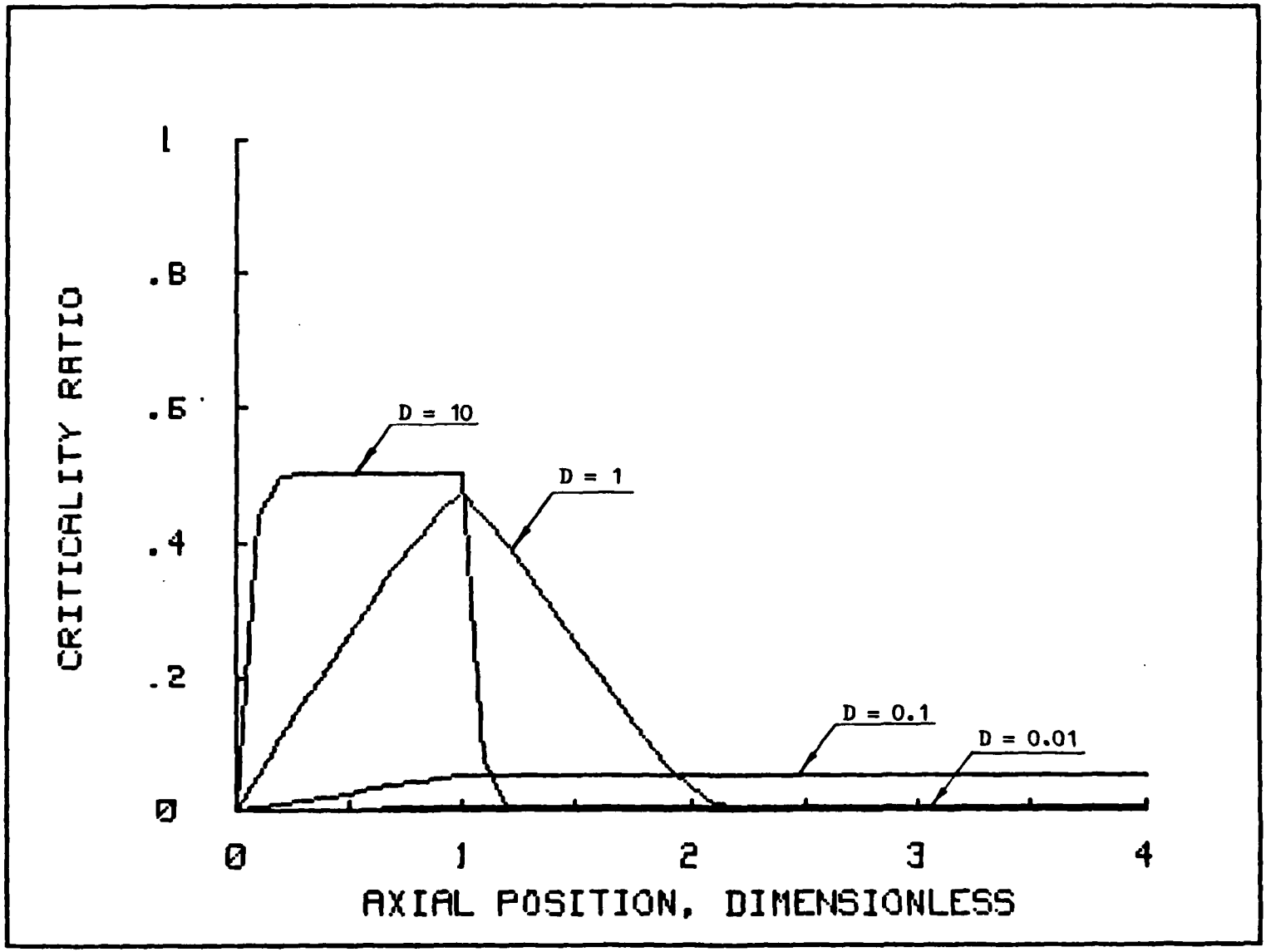

FIGURE 15.

CRITICALITY RATIO AT WINDOW ALONG ITS AXIS FOR VARIOUS DAMKOHLER NUMBERS, EQUIVALENCE RATIO 1.0, RADIATION ENERGY INPUT 0.06 J IN SPECTRAL RANGE 145 TO 245 nm, FILTER: 175 nm LONGPASS CUTOFF

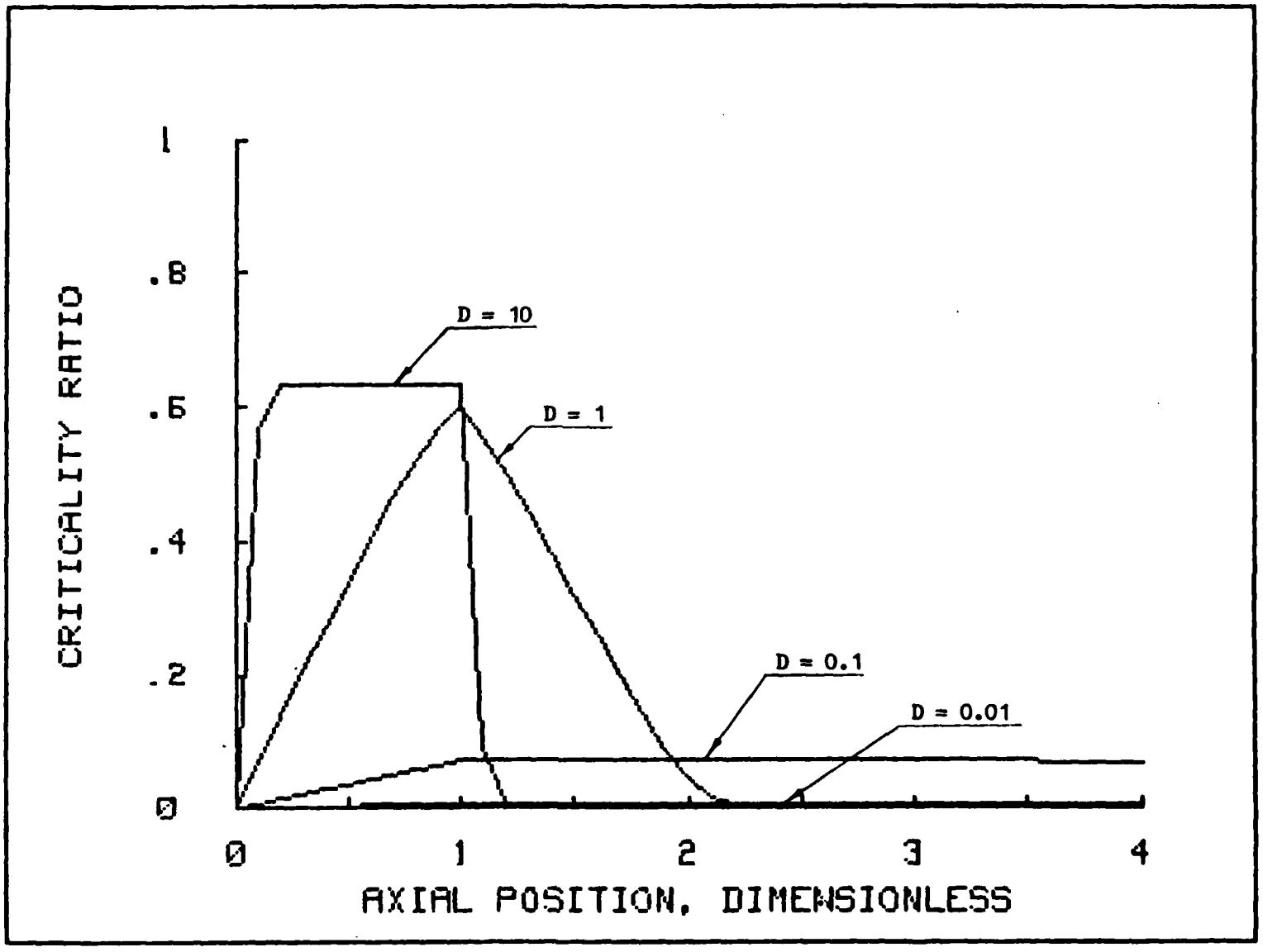

FIGURE 16.

CRITICALITY RATIO AT WINDOW ALONG ITS AXIS FOR VARIOUS DAMKOHLER NUMBERS, EQUIVALENCE RATIO 1.0, RADIATION ENERGY INPUT 0.06 j IN SPECTRAL RANGE 175 TO 245 nm, NO FILTER

Focussing of Figure 12, it becomes clear that for Damkohler numbers greater than unity (velocities less than 75 m/s), the criticality ratio exceeds 30 times the threshold value required for ignition. Furthermore, this value is reached right at the lending edge of the window. When Damkohler number is decreased to 0.1 (750 m/s, supersonic flows), the previously obtained step distribution of the criticality ratio becomes exponential in nature, and the high ratio of 30 is reached only at the trailing edge. For D = 0.01 (velocity of 7500 m/s, hypersonic flows) the criticality ratio drops precipitously to a value of 6 far at the trailing edge. This means that if the required critical density of atomic oxygen for ignition were an order of magnitude larger than the calculated one, (i.e. 1E17 instead of 1E16 atoms/cc), the ILC lamp will not be anymore capable of photochemically igniting this hypersonic mixtures. Thus, for Damkohler numbers of 0.01 and lower (velocities over 7500 m/s) photochemical ignitions become questionable with the currently available ILC lamps. A remedy to this difficulty was discussed earlier, suggesting to increase the VUV power by, for example, shortening the pulse width.

It is interesting to note that if the Damkohler number were zero (velocity is infinity), the criticality ratio would everywhere be zero (no ignition), whereas if it were infinity (velocity is zero, i.e. the static case), the ratio would be a step distribution extending along the entire window. The conclusion drawn from the figure is that even for very low Damkohler numbers (0.1), the ILC lamp should achieved ignition. This conclusion was corroborated by the experimental results reported above.

Figures 17 through 20 show the effect of Damkohler number and equivalence ratio (ϕ) on the maximum criticality ratio achieved at the window for 0.06 j light pulses and no filtering. The criticality ratio is constant for Damkohler numbers above about 0.2, for all the four equivalence ratios (1.2, 1.0, 0.5 and 0.3). However, it increases in value with decreasing equivalence ratio. This is undoubtedly an absorption effect. At standard conditions, as the mixture becomes more fuel-lean, more molecular oxygen is available for photodissociation. This trend with equivalence ratio corresponds to our experimental results reported above, where minimum ignition energy decreased with decreasing equivalence ratio until ϕ = 0.5, then the trend is reversed. This experimental reversal probably results from an increase in the necessary critical number density (i.e. 1E16) at lower equivalence ratios. Although we have taken this number as constant for all equivalence ratios in our model, it must be a function of equivalence ratio at extreme values. Because at very low fuel-lean conditions ignition cannot be achieved and maintained (heat release is less than heat loss). The variation of the critical density with equivalence ratio has not yet been calculated, but it can be calculated by the same methods used in reference 4. This point deserves further investigation.

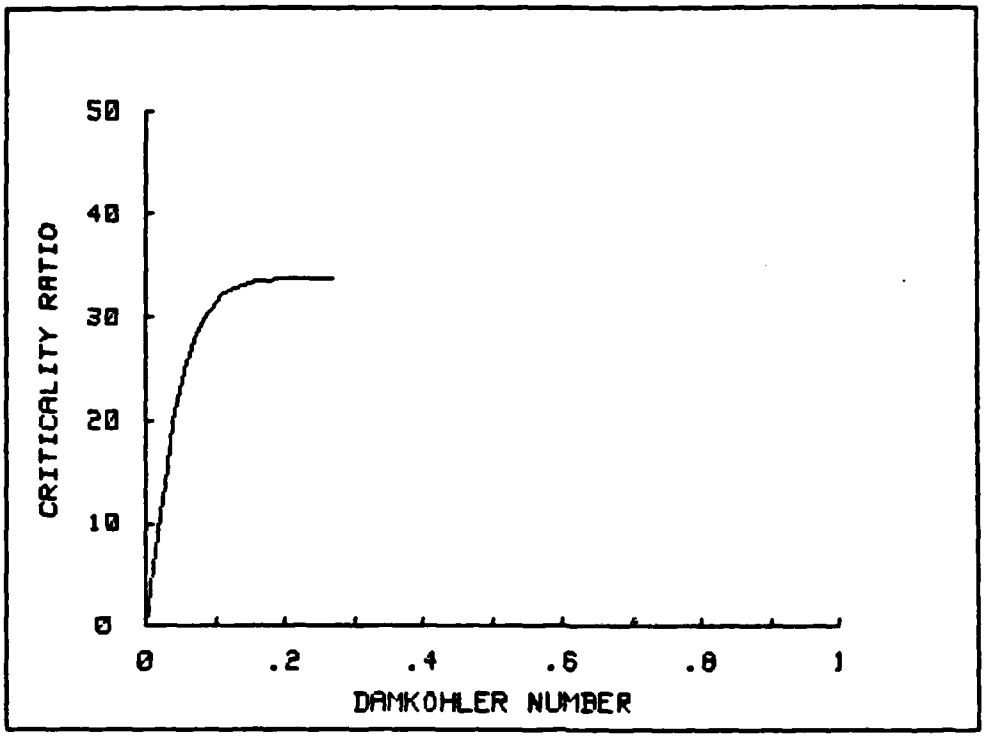

FIGURE 17.

CRITICALITY RATIO AS A FUNCTION OF DAMKOHLER NUMBER, RADIATION ENERGY INPUT 0.06 j, EQUIVALENCE RATIO 1.2

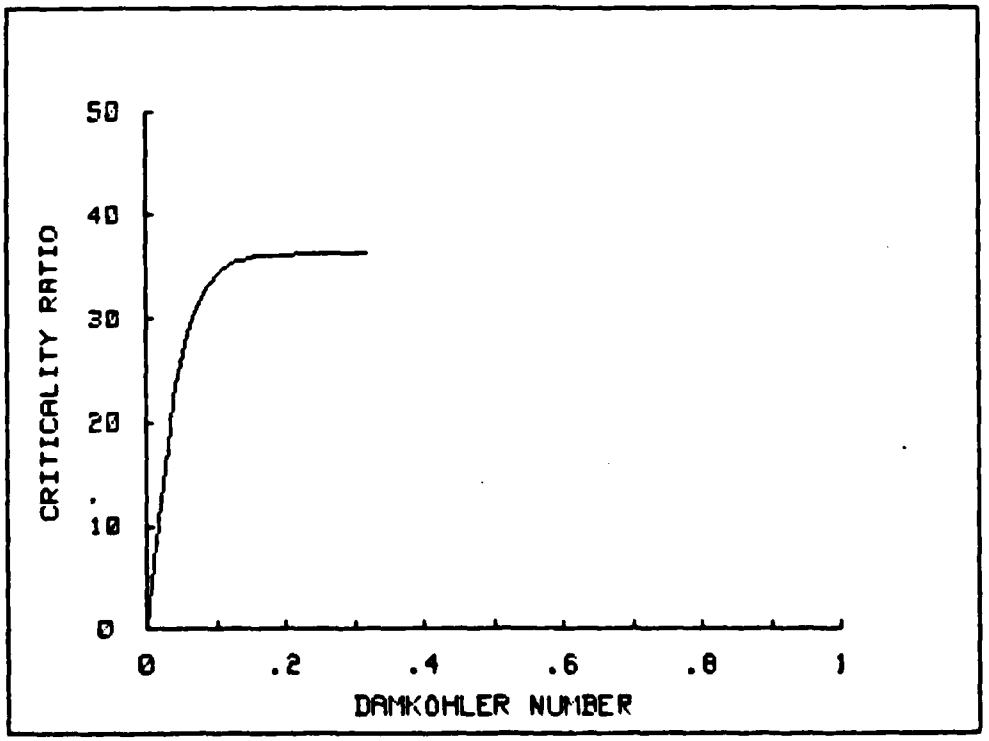

FIGURE 18.

CRITICALITY RATIO AS A FUNCTION OF DAMKOHLER NUMBER, RADIATION ENERGY INPUT 0.06 j, EQUIVALENCE RATIO 1.0

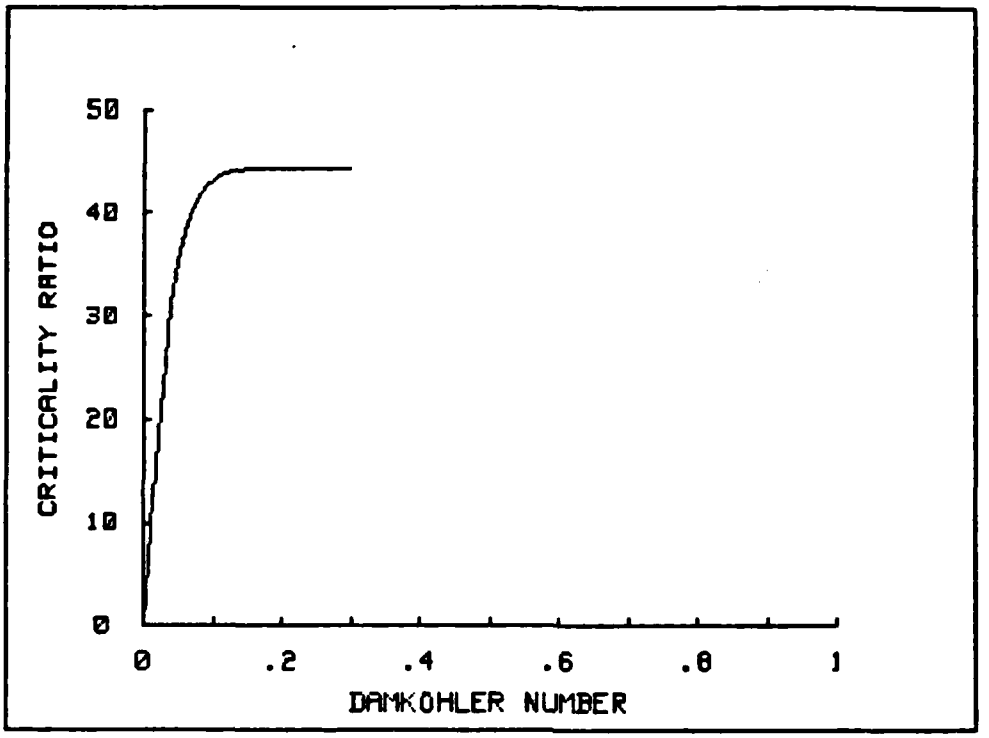

FIGURE 19.

CRITICALITY RATIO AS A FUNCTION OF DAMKOHLER NUMBER, RADIATION ENERGY INPUT 0.06 j, EQUIVALENCE RATIO 0.5

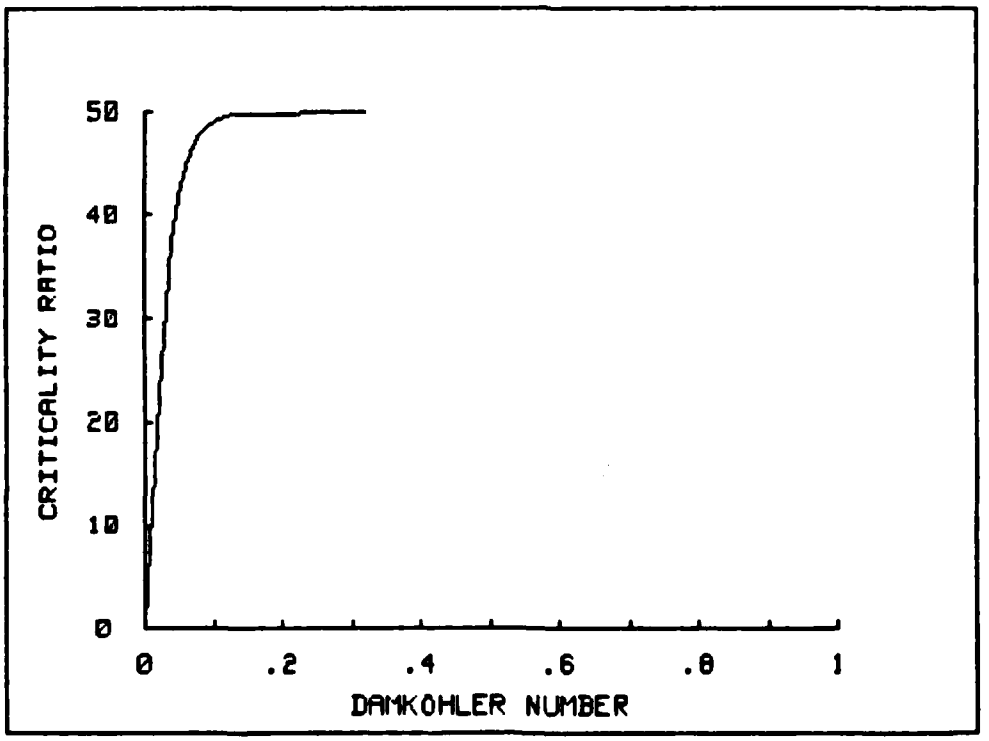

FIGURE 20.

CRITICALITY RATIO AS A FUNCTION OF DAMKOHLER NUMBER, RADIATION ENERGY INPUT 0.06 j, EQUIVALENCE RATIO 0.3

These analytical results are in good conformity with our experimental results and they serve both to explain them and to generalize them. They have accomplished several goals. They have clarified the role of Damkoher number, and demonstrated that the ILC lamp has sufficient output to achieve ignition even at low Damkohler numbers (For D = 0.1, corresponding to supersonic flows). The analytical results have also shown how controlling the spectral distribution of the radiation can control the geometry of the ignition region that is induced in the gas. Finally they have demonstrated that VUV radiative ignition favors fuel-lean mixtures over stoichiometric and fuel-rich mixtures.

2. Radiative Enhancement of Flame Speed

We have continued to use the HCT model to investigate the nature and extent of photochemical enhancement of combustion. In work reported in references (3,5,8), laminar flame speeds were calculated for base cases employing the usual reaction kinetics for H2/air, and for cases in which the photodissociation of either molecular oxygen or the hydroperoxyl radical was simulated. The approach used was to include the unimolecular dissociation reactions (O2 ---> O + O, or HO2 ---> OH + O) with specified rate constants. These results are summarized in Table II or reference (3). The most significant series of runs are those numbered 43 through 48, all at equivalence ratio of 0.4. The base case (Run 43) with no photodissociation gave a flame speed of 47 cm/s. With a rate constant of k = 3 1/s, the inclusion of the reaction O2 ---> O + O throughout the reactor gave a calculated flame speed of 43 cm/s. This lowering of the flame speed was attributed to the presence of H2O2 well ahead of the flame front. The hydrogen peroxide was the end product of the unimolecular dissociation, O2 --> O + O, occurring in the unburned gas. It was thus found necessary to limit this reaction to the flame front. The first attempt at doing so was to include the photodissociation reaction only in those regions (cells of the numerical scheme) in which the temperature was within a specified range, typically ~400 to 700 K. The major finding was that the reaction HO2 ---> OH + O with k = 1E6 1/s gave an increase of flame speed to 60 cm/s. The rate constant was erroneously given in reference (3) as 1E4 1/s. The correct value is 1E6 1/s, as reconfirmed by duplicating the run as Run 75, discussed below. In this case, a substantial increase in the concentrations of O, H, and OH and a significant decrease in HO2 and H2O2 at the flame front were observed.

In order to understand more clearly the role of the photodissociation of O2 and HO2 in combustion enhancement, additional runs of the HCT model suggested by the earlier work have been made. These runs were performed in two groups: earlier runs, designated Series I, and later runs, Series II, made to follow up on the first set. We describe the results and discuss the conclusions drawn from these two groups of runs in order.

The results of the runs of Series I are summarized in Table I; all are at the equivalence ratio of 0.4 at atmospheric pressure. Runs 62 and 70 incorporate the dissociation of HO2 with lower rate constants than the value previously used; 1 1/s and 100 1/s, respectively. The flame speed calculated for Run 62 is 47 cm/s, unchanged from that of the base case with no photodissociation. The value for Run 70 (k = 100 1/s) is between 48 and 49 cm/s. The species profiles for this run are given in Figure 21 (a,b,c,d,e,). Comparison of these profiles with those of the base case given in Figure 8 of reference (3) reveals no essential difference. Thus, the inclusion of the photodissociation with these lower rate constants has no significant effect on flame propagation in the system under consideration, although a slight increase in flame speed is indicated. After these runs, the question of the response of the flame speed to the photodissociative rate constant for HO2 was unanswered. The product radicals of that dissociation participate in several significant reations which in turn produce HO2 (e.g. via chain-branching, and O2 + H + M ---> HO2 + M, see Table I of reference (3). We suspected that this feedback could result in a nonlinear response and proceeded to study the question more fully in the runs of Series II.

Table I

SUMMARY OF SERIES I ENHANCEMENT MODELING RUNS FOR H2/AIR AT ATOMOSPHERIC PRESSURE AND EQUIVALENCE RATIO OF 0.4 USING HCT

Run Number	Simulated Photodissociation	Rate Constant (1/s)	Spatial Extent*	Flame Speed (cm/s)
62	HO2-->OH+O	1	R	47
65	O2 -->O +O	3, increased during run to 30	W:400-700	43
67	O2 -->O +O	300	W:400-700	47
69	O2 -->O +O	3000	W:375-700	51
70	HO2-->OH+O	100	R	48.5

---

*

R = Photodissociation throughout entire reactor
W:T1-T2 = Photodissociation confined to reactor region in which the temperature is between T1 and T2 (K).

FIGURE 21

SPECIES PROFILES FOR RUN 70 OF TABLE I
PHOTODISSOCIATION OF HO2 WITH RATE CONSTANT OF 100 1/s
ABSCISSA IS RELATIVE FLAME POSITION (cm);
SPECIES INDICATED ON GRAPH

(a)

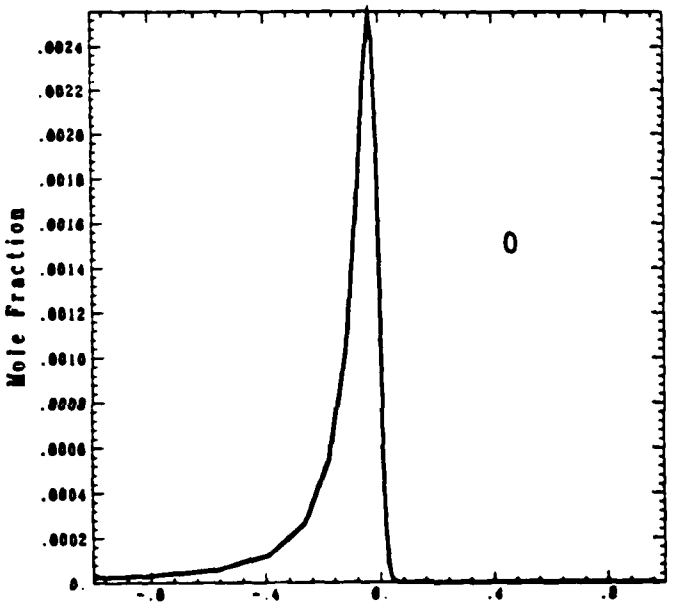

(b)

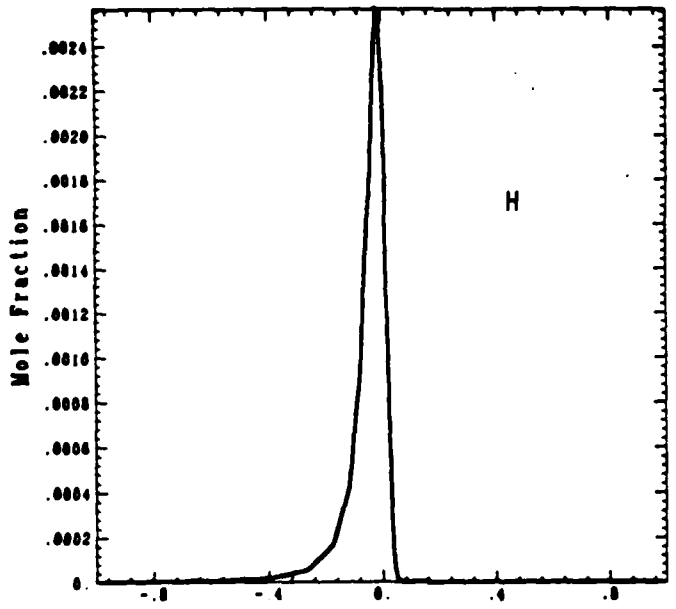

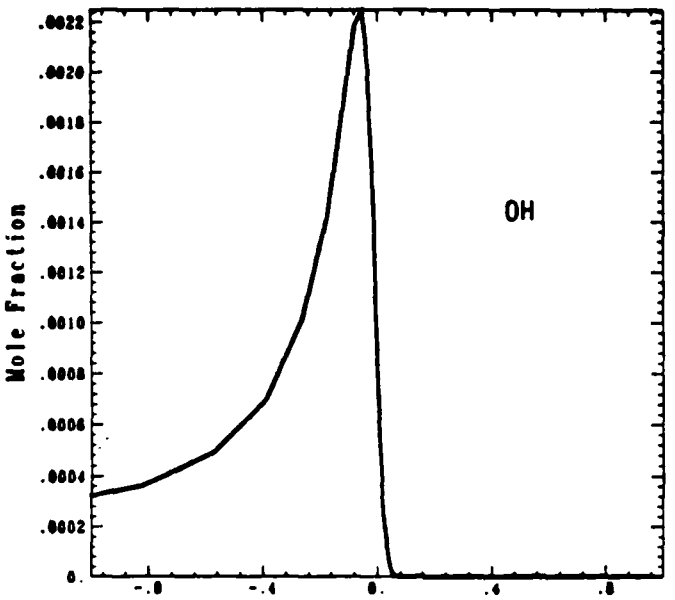

(c)

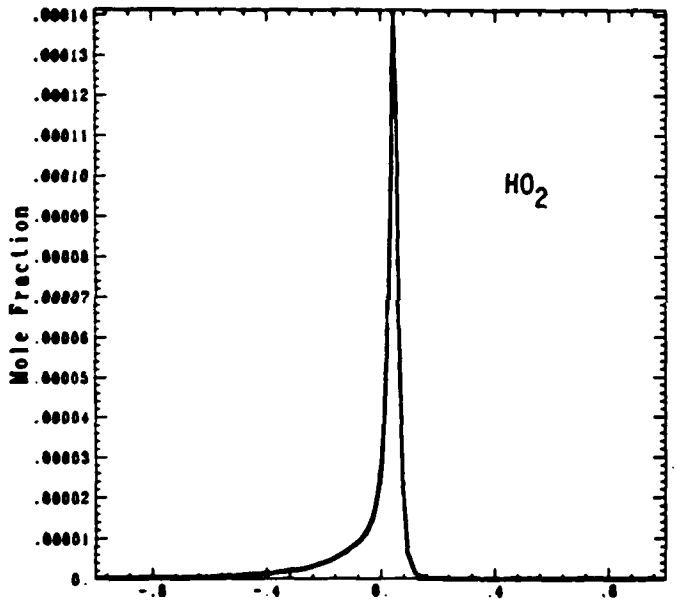

(d)

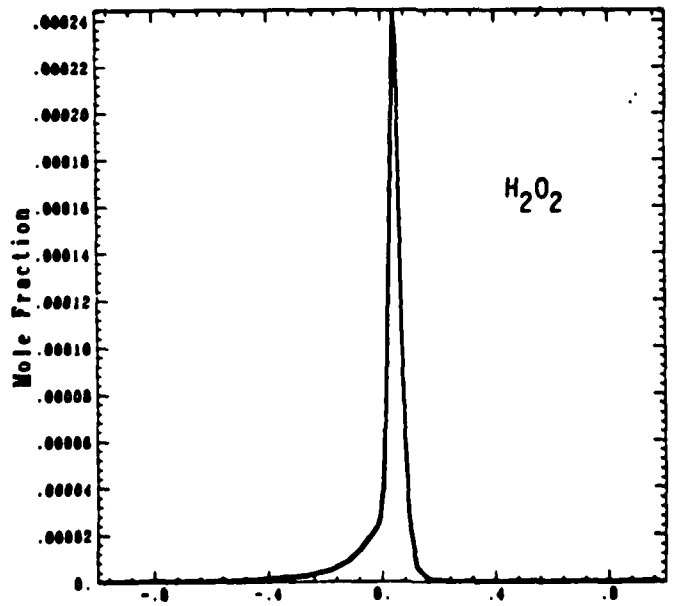

(e)

Figure 21

(continued)

The remaining runs of the first series, numbered 65, 67, and 69, model the photodissociation of molecular oxygen at increasing values of the rate constant. Numerical problems did arise in these cases, associated with the use of a temperature window to limit the reaction to the vicinity of the flame front. For example, with the window set at 400 to 700 K, the zones used in the numerical discretization which were just ahead of the flame convectively heated to a temperature just exceeding the lower limit of the window, thereby turning on the reaction O2 ---> O + O. The resulting oxygen atoms participate in endothermic reactions which in some circumstances lower the temperature sufficiently to shut the dissociation off. This oscillatory behavior caused the automatic time step algorithm of the integrator to require smaller and smaller time steps, eventually resulting in a value below the permissible minimum related to machine precision (5,8). It was found by Dr. Westbrook that this problem could be ameliorated by restarting from a flame which was propagating stably, then turning on the reaction and adjusting the limits of the window. By so doing, it was possible to obtain the final steady flame speed values reported.

We turn now to the results obtained in the oxygen dissociation runs of Series I. Run 65 is similar to Run 44 of Table II of reference (3), but with the temperature window approach which successfully eliminated the presence of O and H2O2 ahead of the flame. With the temperature window of 400 to 700 K, the rate constant was increased from 3 1/s to 30 1/s during the run. The flame speed stabilized to approximately 43 cm/s. The species profiles for this run are not presented here because they are essentially identical to those for the base case given in Figure 7 of reference (3). Again, it appears that the inclusion of the unimolecular dissociation of O2, at these rates and with the spatial distribution imposed by the temperatue window used, does not significantly alter species concentrations, but does lower the calculated flame speed from the base case value of 47 to 43 cm/s.

In Run 67, the rate constant was further increased to 300 1/s, with a return of the flame speed to the base case value of 47 cm/s. Species profiles for this run are displayed in Figure 22 (a,b,c,d,e). Several differences are evident between these profiles and those of run 43 (shown in Figure 7 of reference (3); comparison with those in Figure 21 of this document is helpful becuase they are essentially identical to those of the base case). Slightly ahead of the flame, a second peak has appeared in the oxygen atom profile which is undoubtedly due to the inclusion of the unimolecular O2 ---> O + O with a temperature window. Examination of the temperature profile (not shown) reveals that the position of the shoulder coincides with the region in which the mixture temperature is between 400 and 700 K. The larger peak coincides in position with the conventional peak exhibited in the base case, but its peak value is lower, the mole fraction dropping from approximately 0.0024 to 0.0018. The profiles of the remaining species plotted (OH, H, HO2, and H2O2)

FIGURE 22

SPECIES PROFILES FOR RUN 67 OF TABLE I
PHOTODISSOCIATION OF O2 WITH RATE CONSTANT OF 300 1/s
ABSCISSA IS RELATIVE FLAME POSITION (cm);
SPECIES INDICATED ON GRAPH

(a)

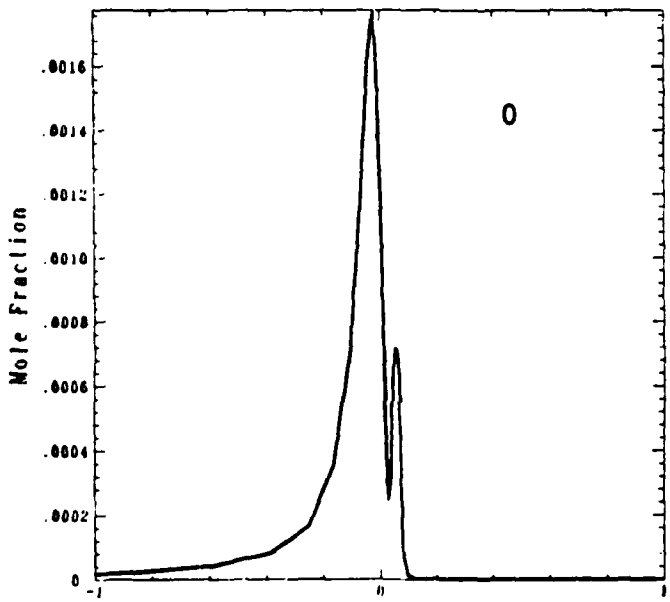

(b)

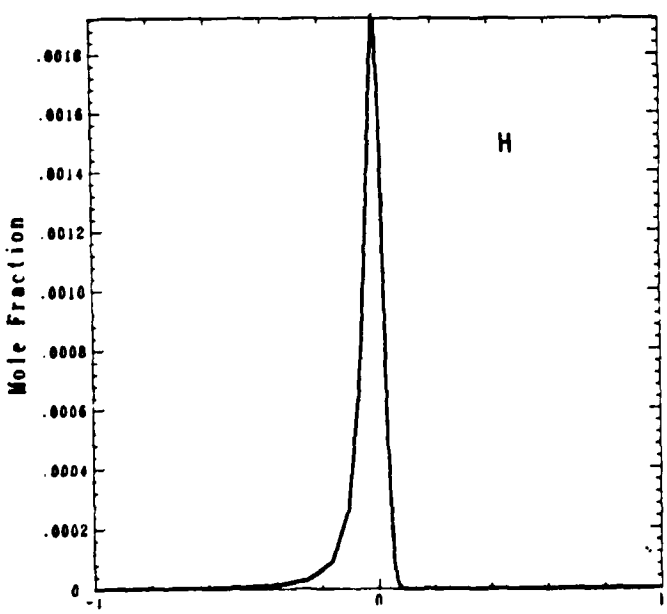

(c)

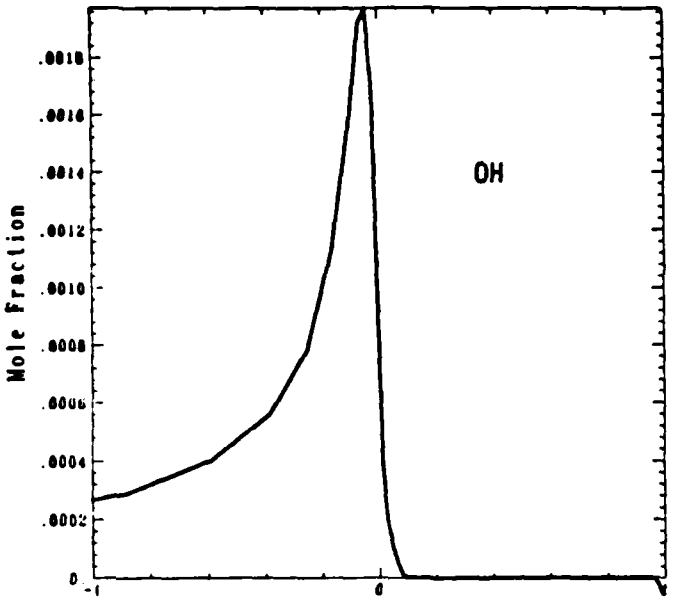

(d)

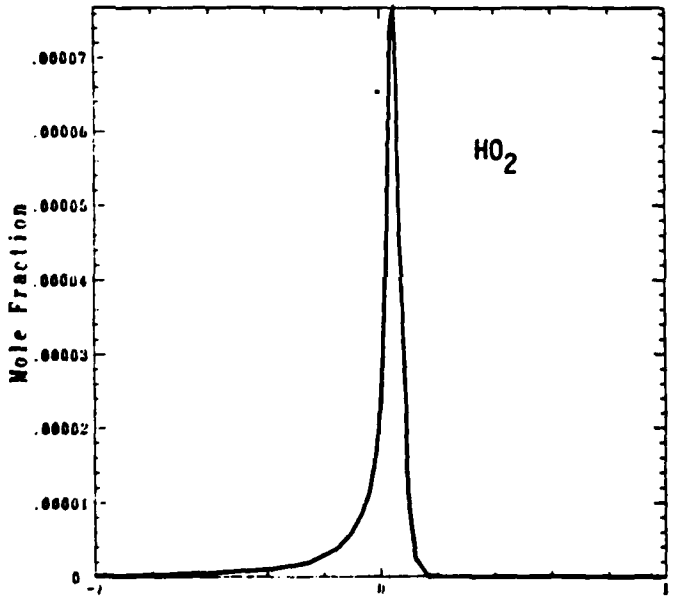

(e)

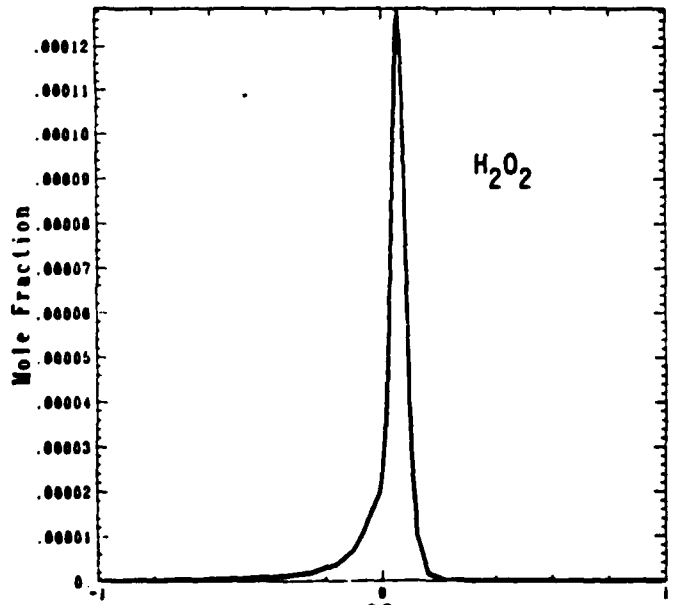

Figure 22

(continued)

have retained the same shape and position relative to the flame, but peak concentrations are lowered in all cases. It appears that atomic oxygen at this level and with the indicated spatial distribution with respect to the flame front is driving the reactions to completion with lower concentrations of radicals and intermediates, without appreciably changing the flame of speed.

We now examine the results of Run 69 with the rate constant further increased to 3000 1/s, for O2 ---> O + O, giving a flame speed of 51 cm/s. This is an increase of approximately 9% over the base case. The species profiles are given in Figure 23 (a,b,c,d,e). Again the oxygen atom profile differs from that of the base case by the presence of a second peak ahead of the flame front stemming from the high rate of unimolecular dissociation of molecular oxygen at the temperature window. In this run, however, the second peak has a maximum value much greater than that of the conventional peak occuring in the same relative position as in Run 67, due to the higher rate constant. The narrowness of the second peak, as the case also for Run 67, is due to the fact that the mixture temperatue rapidly exceeds the upper limit of the temperature window and does so at the point at which the peak subsides. The other (conventional) peak which follows this induced peak is due to the usual reaction pathways, but has a much lower maximum concentration than the corresponding peak of the base case (mole fraction of approximately 0.0018 compared to 0.0024). This lowering of peak values can also be seen to occur for all the other profiles. The maximum values do correspond to those obtained in Run 67, except for H2O2, can be seen to have been translated slightly to the post-flame side of the central flame position indicated by zero and defined from the location of the zone of maximum energy deposition. It is evident that peak concentrations of OH, H, and even O at the flame center are lower in Run 69 than in the base case, and yet the calculated flame speed has increased.

From these runs it was not possible to distinguish the effects due to the value of the dissociative rate constant and those due to the choice of temperature window. It appeared that the peak in oxygen atom concentration ahead of the flame front was an artifact due to the low value selected for the upper limit of the temperature window. More important, from photochemically simulated runs in which the atomic oxygen level was actually lower at the flame front than in the base case, we believed that its presence was not consistent with the objective of combustion enhancement. We resolved to study this question more thoroughly in a second set of runs, designated here as Series II.

The results from Series II are summarized in Table II. We begin by discussing those runs which model the photodissociation of HO2. For these cases no temperature window is required because the absorbing species, HO2, is present only at the flame front. These runs will be considered in the order: Numbers 73, 74, 76, and 75; with increasing value of the rate constants: 1E4, 1E5, 5E5 and 1E6 1/s, respectively.

FIGURE 23

SPECIES PROFILES FOR RUN 69 OF TABLE I
PHOTODISSOCIATION OF O2 WITH RATE CONSTANT OF 3000 1/s
ABSCISSA IS RELATIVE FLAME POSITION (cm);
SPECIES INDICATED ON GRAPH

(a)

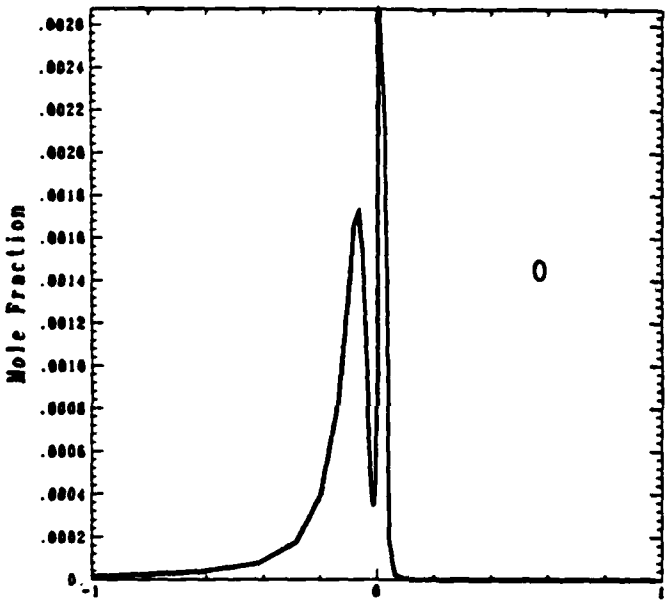

(b)

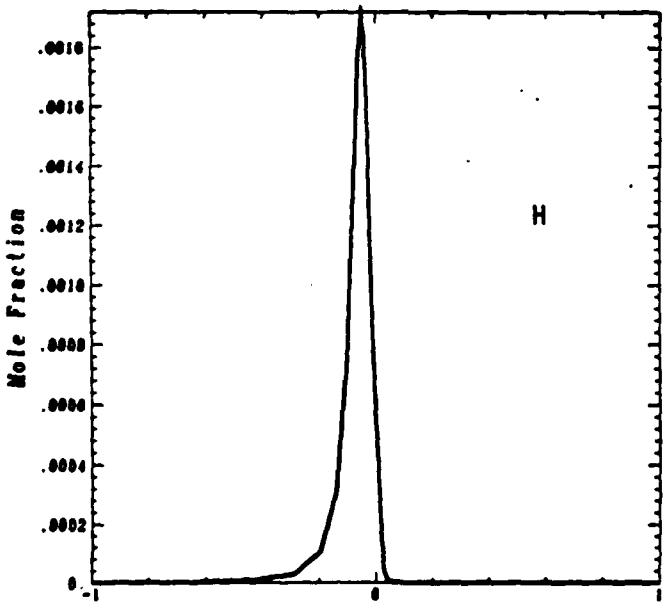

(c)

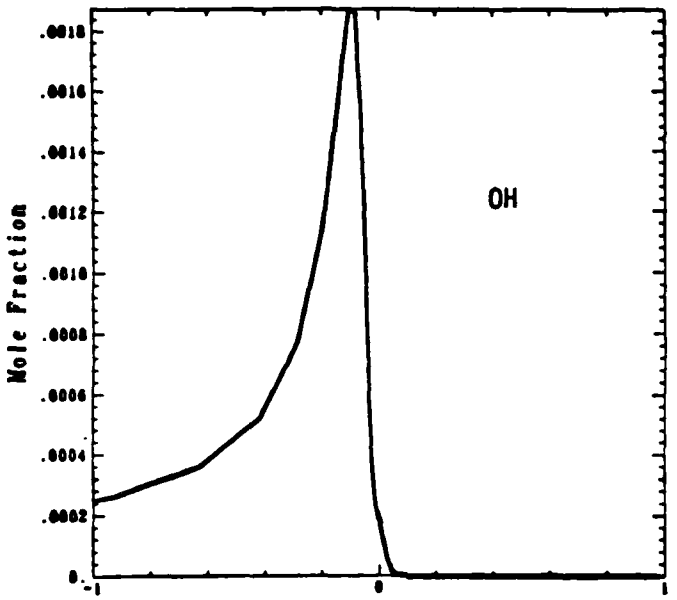

(d)

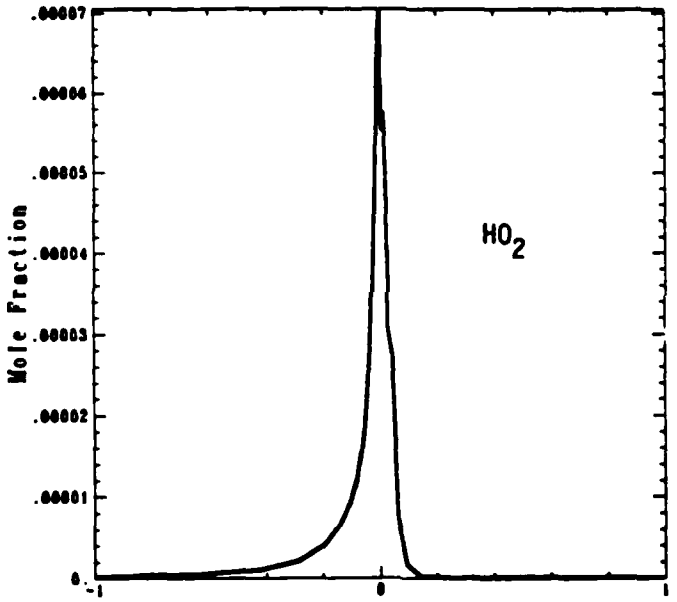

(e)

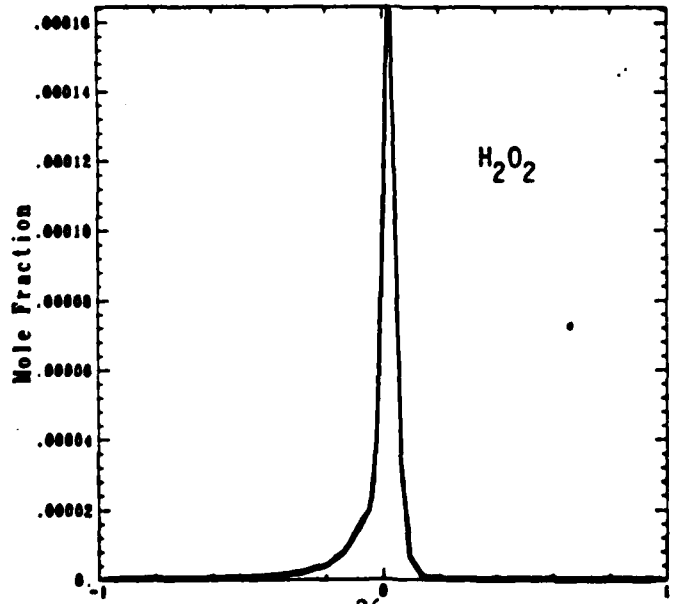

Figure 23

(continued)

TABLE II

SUMMARY OF SERIES II ENHANCEMENT RUNS FOR H2/AIR
AT ATMOSPHERIC PRESSURE AND EQUIVALENCE RATIO OF 0.4 USING HCT

Run Number	Simulated Photodissociation	Rate Constant (1/s)	Spatial Extent*	Flame Speed (cm/s)
72	O2 -->O + O	3E3	W:375-1300	76
73	HO2-->OH+ O	1E4	R	48.5
74	HO2-->OH+ O	1E5	R	50.5
75	HO2-->OH+ O	1E6	R	60.5
76	HO2-->OH+ O	5E5	R	56.5
77	O2-->O + O	3E2	W:375-1300	55
78	O2-->O + O	1.2E3	W:375-1300	66

---

*
R = Photodissociation throughout entire reactor
W:T1-T2 = Photodissociation confined to reactor region in which the temperature is between T1 and T2 (K).

The calculated flame speed for Run 73 is 48.5 cm/s, an insignificant increase (3%) over the flame speed of 47 cm/s obtained in the base case, (Run 43, Ref. 3). This result is similar to that obtained for Run 70 with a lower rate constant of 1E2 1/s. The species profiles are also virtually identical to those of Run 70 (Figure 21), and thus are not presented here. However, despite the similarity this run is important in determining the minimum threshold rate constant (i.e. VUV intensity) above which a radiative effect begins to play a dominate role in enhancing the flame speed. This is corroborated by examining Run 74. The rate constant is increased by an order of magnitude (from 1E4 to 1E5) and the flame speed is 50.5 cm/s, an increase of approximately 7% over the base case velocity. When the species profiles (dashed curves) are compared to those of the base case (solid curves) in Figure 24 (a,b,c,d,e), the readily discernible difference is that the HO2 and H2O2 peaks are diminished. The inclusion of the unimolecular dissociation HO2 --> OH + O explains the lower concentration of HO2. Considering the other species, we observe that the peak concentration of each of the fast radicals (O,H,OH) in the base case is approximately twenty times the peak concentration of HO2. We would, therefore, not expect to see major changes in these profiles, even if HO2 would be completely photodissociated. Close examination of them

FIGURE 24

SPECIES PROFILES FOR RUN 74 TABLE II
SOLID CURVES-BASE CASE, NO PHOTODISSOCIATION
DASHED CURVES-PHOTODISSOCIATION OF HO2 WITH RATE CONSTANT 1E5 1/s
ABSCISSA IS RELATIVE FLAME POSITION (cm);
SPECIES INDICATED ON GRAPH

(a)

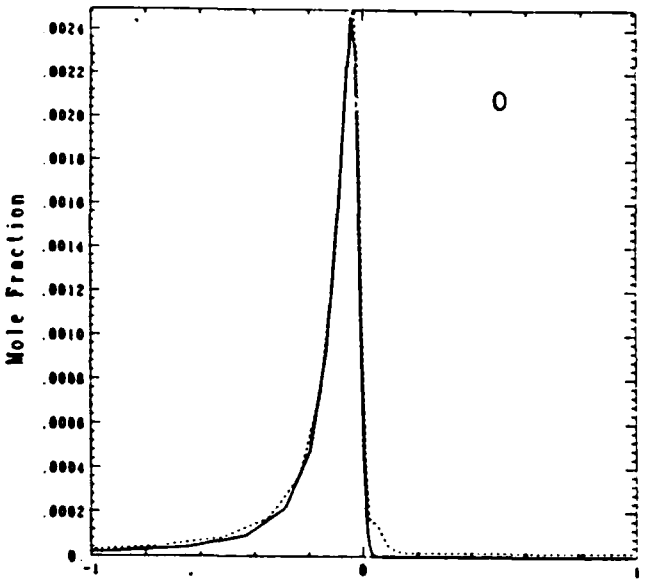

(b)

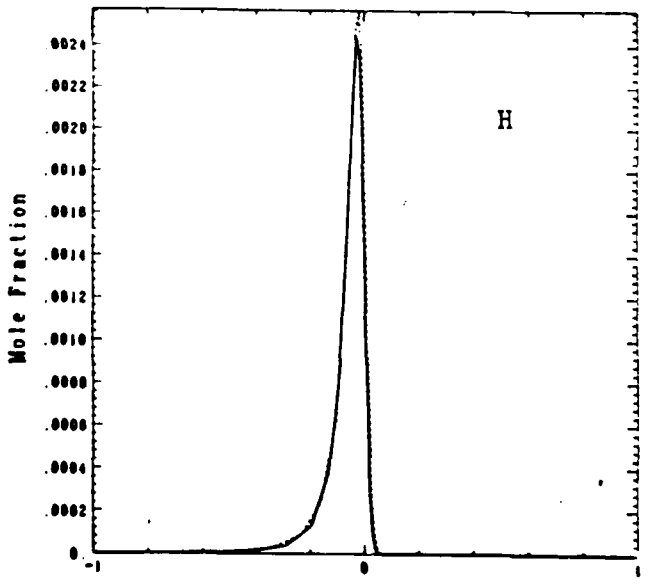

(c)

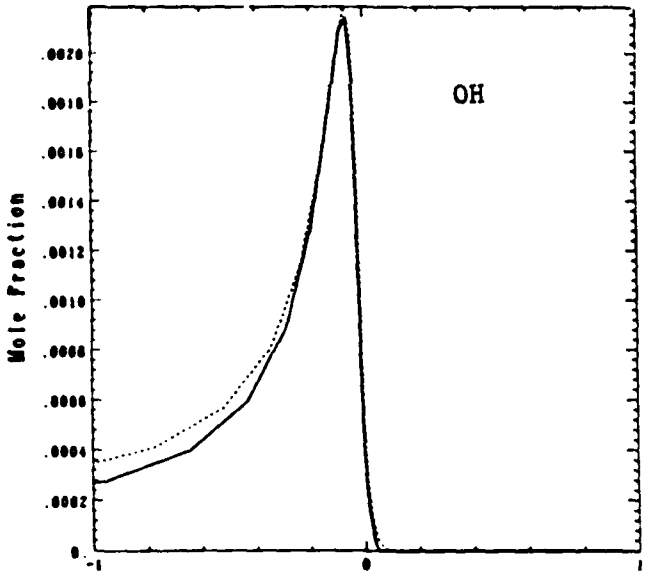

(d)

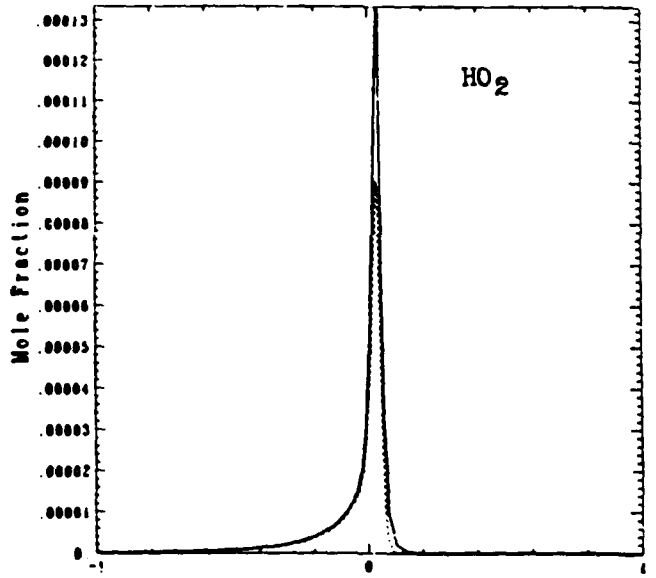

(e)

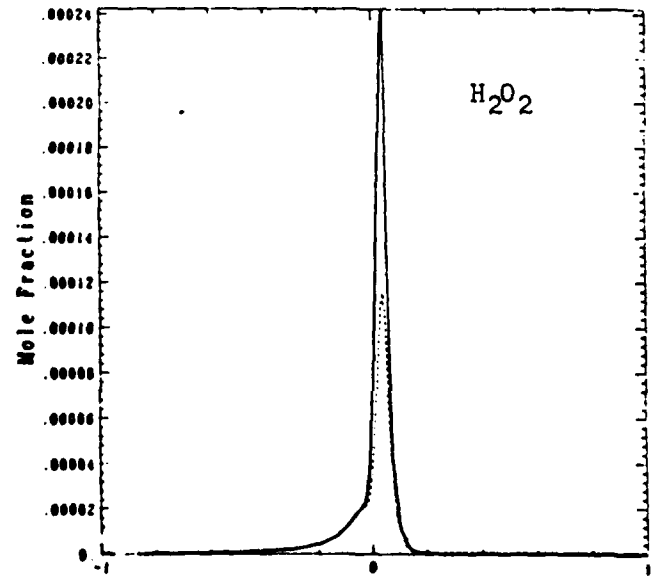

Figure 24

(continued)

does reveal that, with the dissociation of HO2, their maximum concentrations are slightly increased. Moreover, a small shoulder has appeared on the oxygen atom profile at a position slightly ahead of the flame front which coincides with the location of the HO2 peak and at which the hydroxyl radical concentration is slightly increased. These somewhat elevated radical levels result in a decreased concentration of hydrogen peroxide via such reactions as H2O2 + O ---> H2O + O2; H2O2 + H ---> H2O + OH; and H2O2 + OH ---> H2O + HO2.

The observations just made for Run 74 apply as well for Runs 76 and 75 with rate constants 5E5 and 1E6 1/s, respectively. The profiles for these cases are found in Figures 25 and 26 (a,b,c,d,e), respectively. Due to the increased value for the rate constant, the changes in species profiles from those of the base case are more dramatic. The HO2 and H2O2 peaks diminish and the O, H, and OH peaks enlarge as the rate constant is increased. The shoulder on the oxygen atom profile has become a small peak in Run 76 and a more pronounced peak in Run 75.

Most importantly, the greater rate of HO2 photodissociation has also increased the calculated flame speed to 56-57 cm/s (the best bracketing values which can be determined from the run; 56.5 cm/s is used for comparison) for Run 76 and to 60.5 cm/s for Run 75. The photodissociation of the hydroperoxyl radical evidently results in circumventing ("short-circuiting") the radical terminating pathways leading to HO2 and H2O2, and results in a significant increase in flame speed. We have summerized all the flame speed values for the HO2 runs in Table III. A change in the rate constant from 1E2 1/s to 1E4 1/s to 1E5 1/s produces a modest improvement in the increase over base case velocity from 3% to 7%; whereas the further increase to 5E5 1/s gives a considerable gain of 20%. With the value 1E6 1/s, the flame speed shows a substantial increase of 29% over the base case value. This nonlinear response of the flame speed to the rate of dissociation suggests a threshold for significant enhancement due to a feedback in which the product radicals participate in several significant reactions which in turn produce HO2. It is not clear how much further the trend toward increased flame speed will continue; undoubtedly at some value the HO2 would be depleted so rapidly that no further increase in flame speed would be achieved. This value is yet to be determined.

We now examine the results of the recent runs modeling the photodissociation of molecular oxygen. As discussed above, we suspected that the temperature window of ~400 to 700 K (3,5,8), used to limit the photodissociation reaction to the flame front in the first series of runs, had not been well chosen. In fact, by producing a spike in the oxygen atom concentration too far ahead of the flame, the concentration of radicals at the flame front had actually been reduced, giving either no enhancement (Run 67) or even a retardation (Run 65) of the flame speed. We determined to make a series of runs with a higher limit for the temperature window. The previously encountered numerical

FIGURE 25

SPECIES PROFILES FOR RUN 76 TABLE II
SOLID CURVES-BASE CASE, NO PHOTODISSOCIATION
DASHED CURVES-PHOTODISSOCIATION OF HO2 WITH RATE CONSTANT 5E5 1/s
ABSCISSA IS RELATIVE FLAME POSITION (cm);
SPECIES INDICATED ON GRAPH

(a)

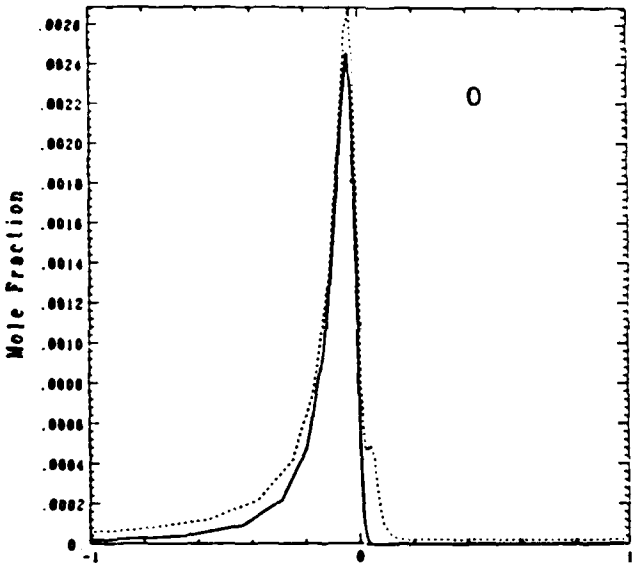

(b)

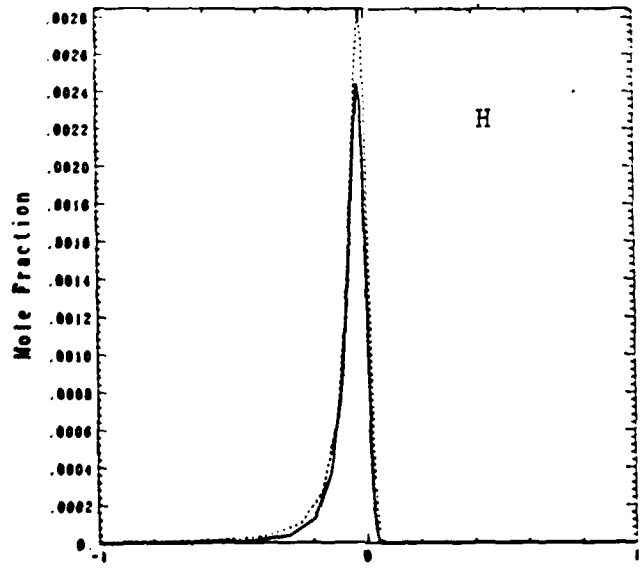

(c)

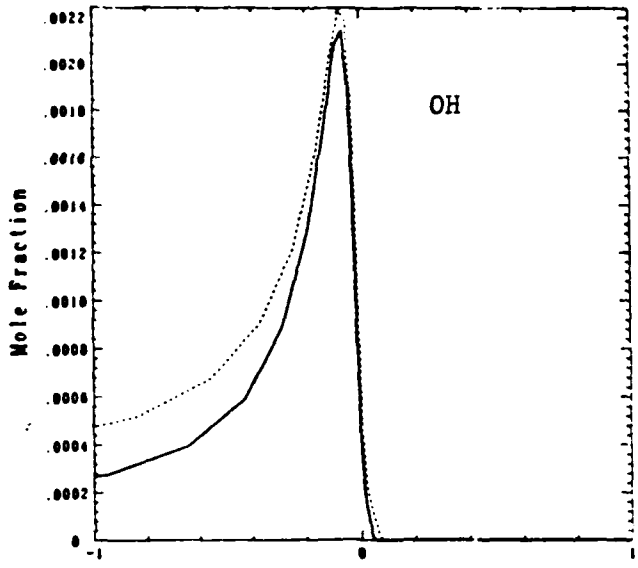

Figure 25

(continued)

(d)

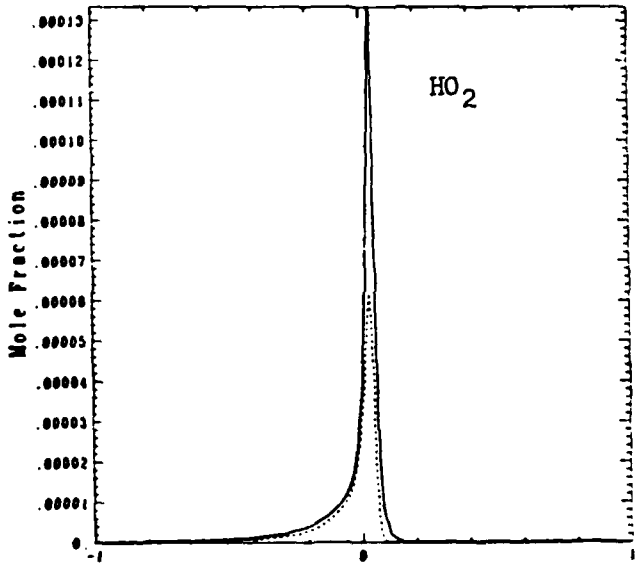

(e)

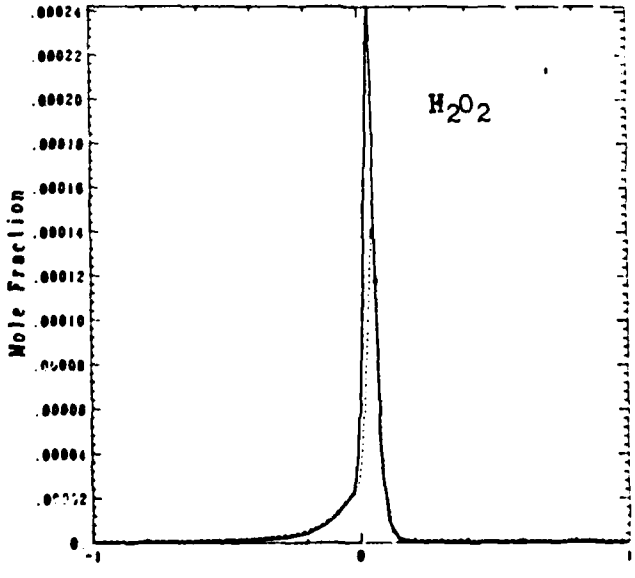

FIGURE 26

SPECIES PROFILES FOR RUN 75 TABLE II
SOLID CURVES-BASE CASE, NO PHOTODISSOCIATION
DASHED CURVES-PHOTODISSOCIATION OF HO2 WITH RATE CONSTANT 1E6 1/S
ABSCISSA IS RELATIVE FLAME POSITION (cm);
SPECIES INDICATED ON GRAPH

(a)

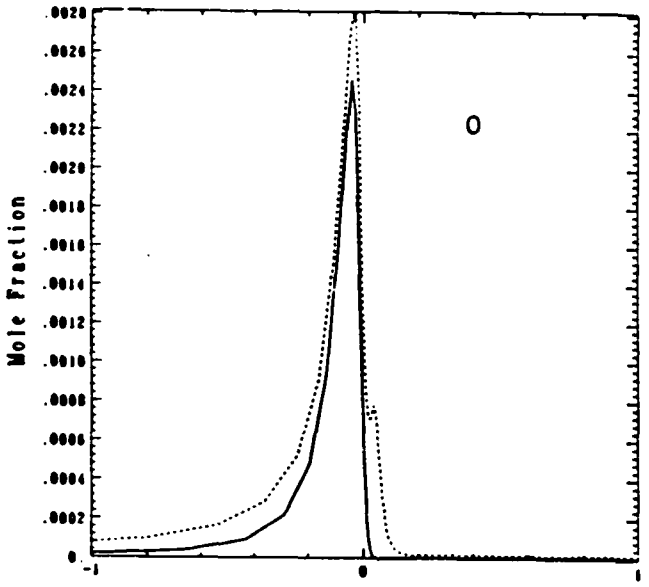

(b)

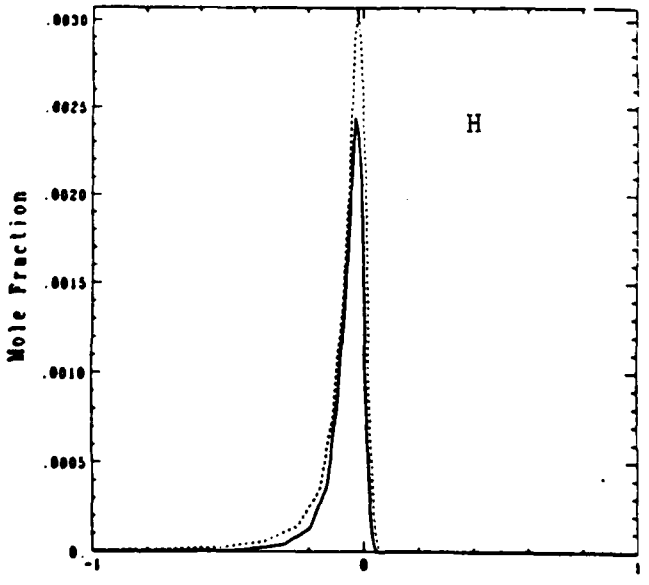

Figure 26

(continued)

(c)

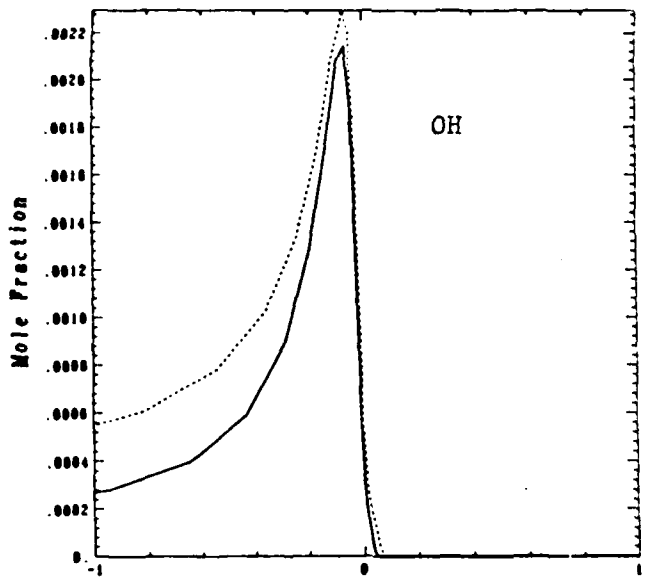

(d)

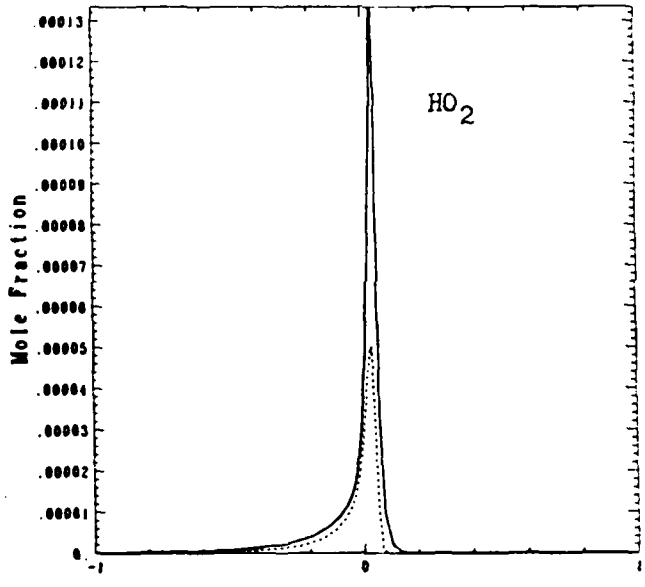

(e)

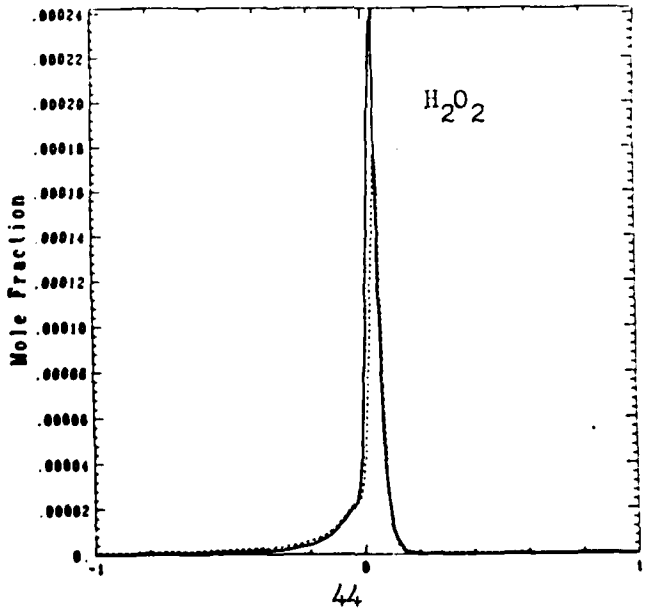

TABLE III

INCREASE IN FLAME SPEED VERSUS
DISSOCIATIVE RATE CONSTANT FOR HO2

Rate Constant (1/s)	Calculated Flame Speed (cm/s)	Increase Over Base Case (%)
0	47	-(Base Case)
1	47	-
1E2	48.5 (48-49)	3
1E4	48.5 (48-49)	3
1E5	50.5	7
5E5	56.5 (56-57)	20
1E6	60.5	29

difficulties again occurred. Dr. Westbrook arranged for the kinetics module of the HCT program to be modified so that the modeled reaction is brought on more smoothly. This modification resolved the time-step difficulty and allowed the desired results to be obtained more easily than before.

The first of the O2 runs we discuss is Run 72 which showed the most significant enhancement with a calculated flame speed of 76 cm/s, an increase of 29 cm/s over the base case, of 47 cm/s. This represents a profound enhancement of 62% (!). The temperature window used was 375 to 1300 K. The upper limit of 1300 K was chosen to extend the modeled photodissociation, O2 ---> O + O, sufficiently far into the flame front so that the two separate peaks encountered in Runs 67 and 69 would coalesce into a single peak. Yet the reaction would not extend into the post-flame region and distort the equilibrium reached.

From the species profiles for this run presented in Figure 27 (a,b,c,d,e), it can be seen that this goal was achieved. With 3000 1/s as the rate constant, the peak oxygen atom concentration has nearly doubled and the peak has broadened considerably. As expected, through chain-branching reactions the higher concentration of oxygen atoms has almost doubled the peak of hydrogen atom concentration, and has increased the maximum concentration of the hydroxyl radical. The position of all of these peaks has been displaced slightly toward the burnt-gas side compared to the base case, presumably due to the temperature

FIGURE 27

SPECIES PROFILES FOR RUN 72 TABLE II
SOLID CURVES-BASE CASE, NO PHOTODISSOCIATION
DASHED CURVES-PHOTODISSOCIATION OF O2 WITH RATE CONSTANT 3E3 1/S
ABSCISSA IS RELATIVE FLAME POSITION (cm);
SPECIES INDICATED ON GRAPH

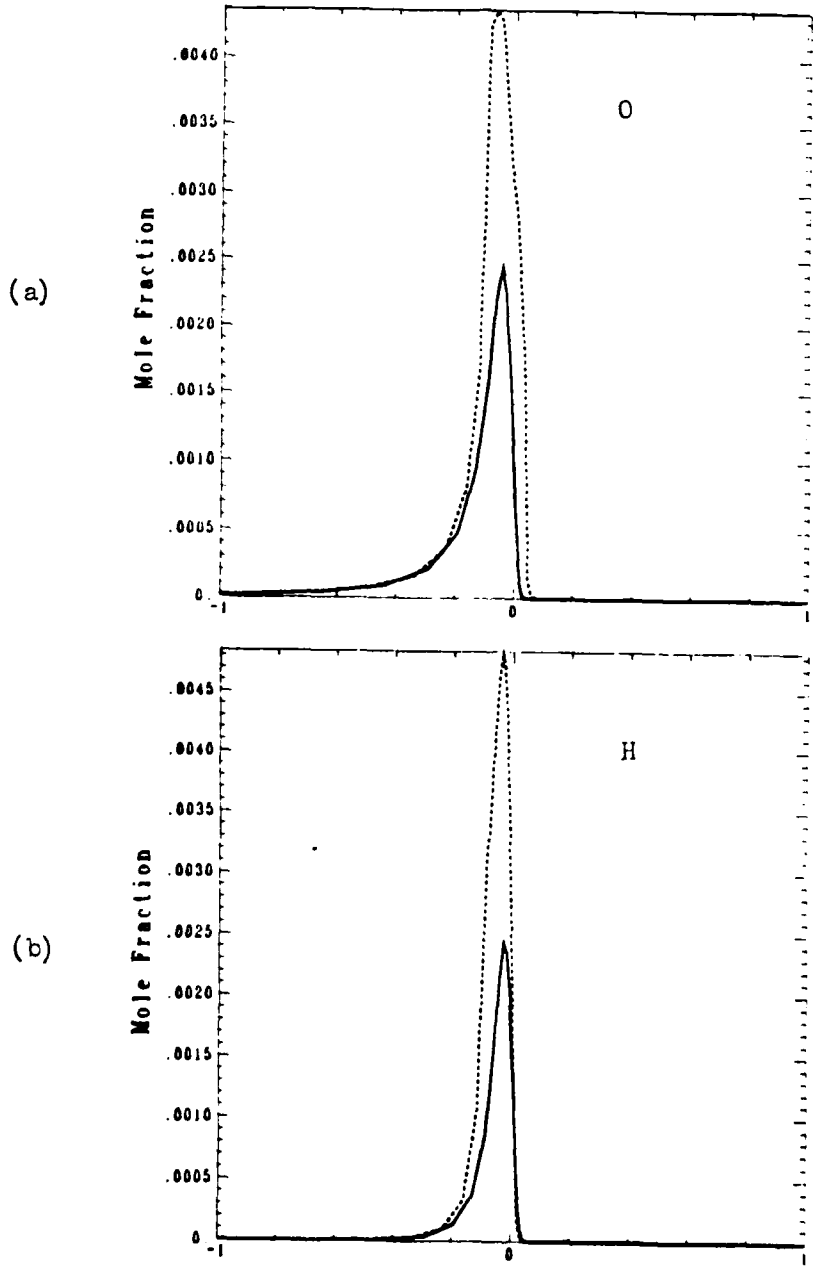

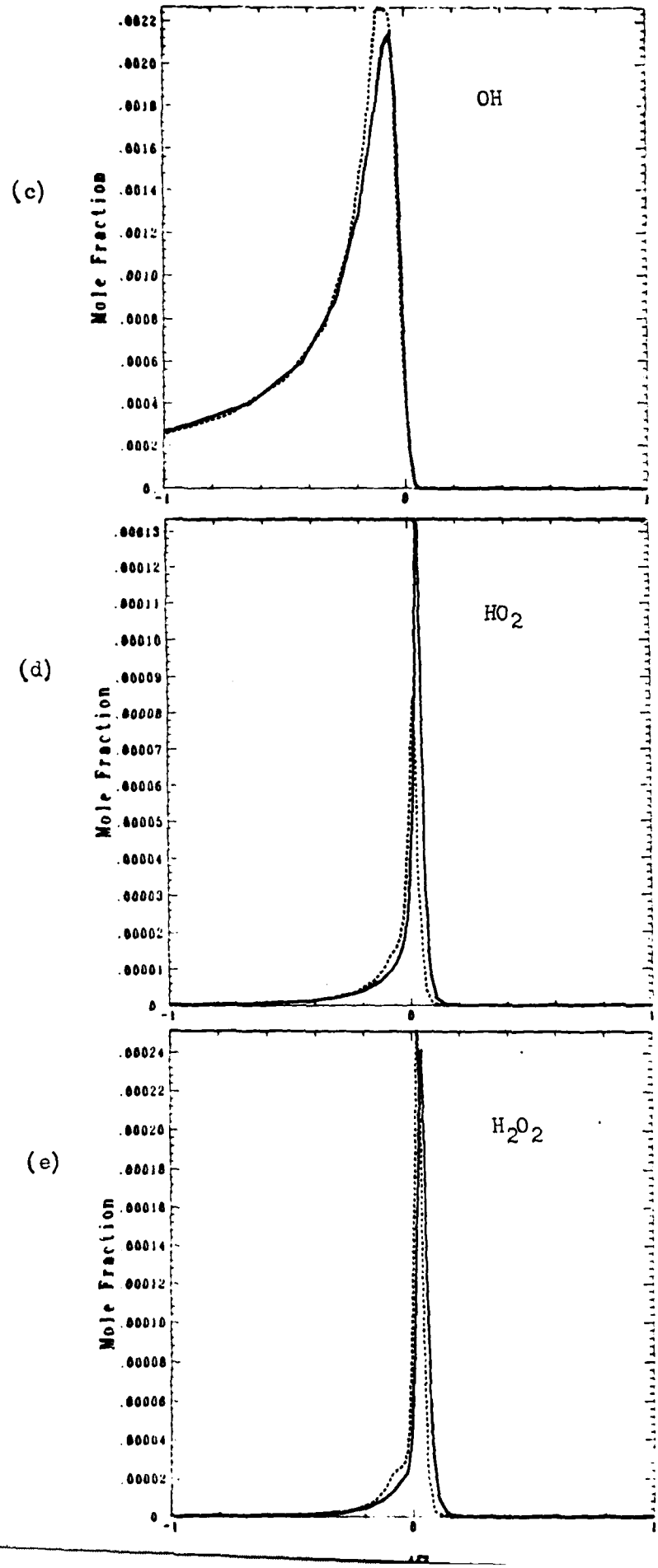

Figure 27

(continued)

window chosen. As for other cases, the increased concentration of fast radicals has reduced the concentration of HO2. Unlike other cases, the hydrogen peroxide profile is not changed appreciably, but is displaced toward the burnt gas with the appearance of a small shoulder on that side. The overlap of the enhanced fast radical pool with the location of increasing water production undoubtedly accounts for these changes (via, e.g., H2O + OH ---> H2O2 + H).

The most notable result from Run 72 is the dramatic increase of 62% in calculated flame speed produced by the increased concentration of radicals at the flame front. This result is especially significant when one compares the 76 cm/s obtained to the value of 51 cm/s calculated for Run 69. The only difference between these two runs is the temperature window used, a point to which we shall return below. Table IV summerizes the increase in flame speed obtained for this run and subsequent other recent O2 runs. It is instructive to compare these results to those of HO2 runs shown in Table III.

TABLE IV

INCREASE IN FLAME SPEED VERSUS
DISSOCIATIVE RATE CONSTANT FOR O2

Spatial Extent; Temperature Window 375-1300 K

Rate Constant (1/s)	Calculated Flame Speed (cm/s)	Increase Over Base Case %
0	47	-- (Base Case)
3E2	55	17
1.2E3	66	40
3E3	76	62

In Run 78, the value for the rate constant for the dissociation of O2 was reduced to 1200 1/s. The flame speed obtained decreased from that obtained for Run 72 to 66 cm/s, still an increase of 40% over the base case value (See Table IV above). The profiles, shown in Figure 28 (a,b,c,d,e), are similar to those of Run 72. As expected, the peak of the oxygen atom concentration is lower than in that run but still increased over the base case. A small shoulder is evident on the unburnt-gas side of the peak, commencing at the lower limit of the temperature window. The HO2 profile also resembles that for Run 72, but the hydrogen peroxide peak is further decreased (below the base case value), not having the copious supply of radicals to enlarge it.

FIGURE 28

SPECIES PROFILES FOR RUN 78 TABLE II
SOLID CURVES-BASE CASE, NO PHOTODISSOCIATION
DASHED CURVES-PHOTODISSOCIATION OF O2 WITH RATE CONSTANT 1.2E3 1/S
ABSCISSA IS RELATIVE FLAME POSITION (cm);
SPECIES INDICATED ON GRAPH

(a)

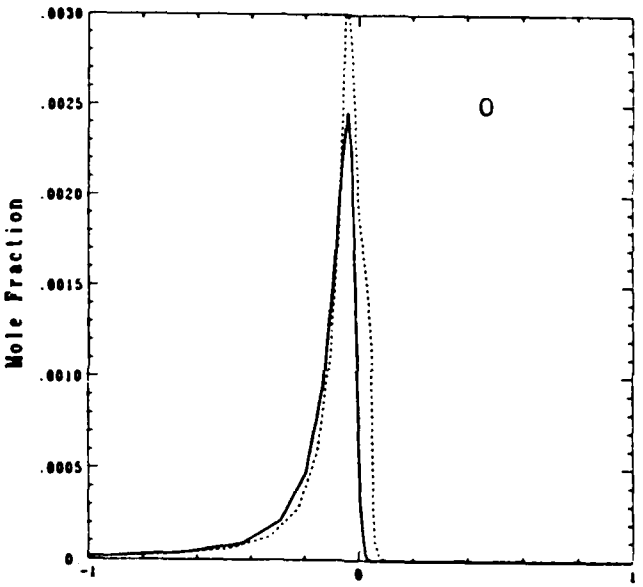

(b)

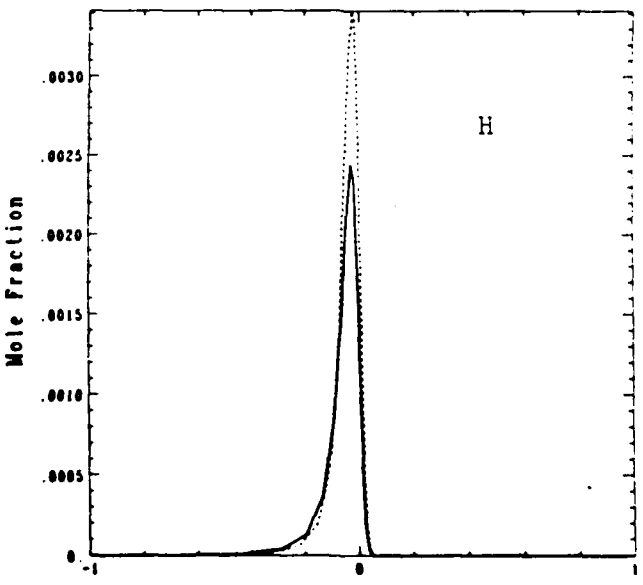

(c)

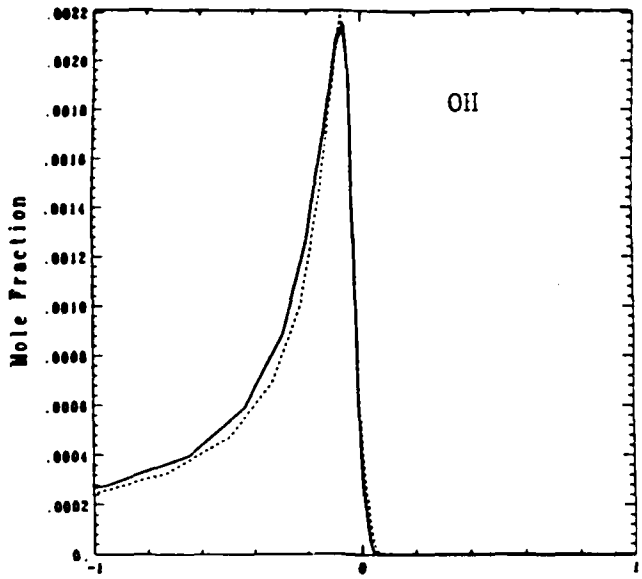

Figure 28

(continued)

(d)

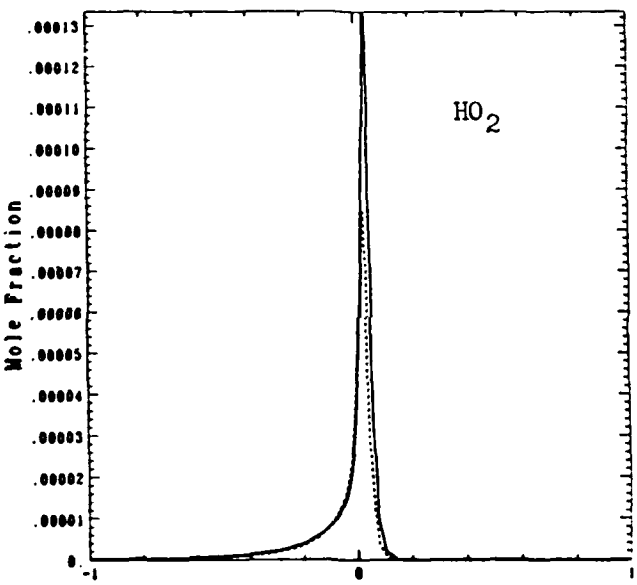

(e)

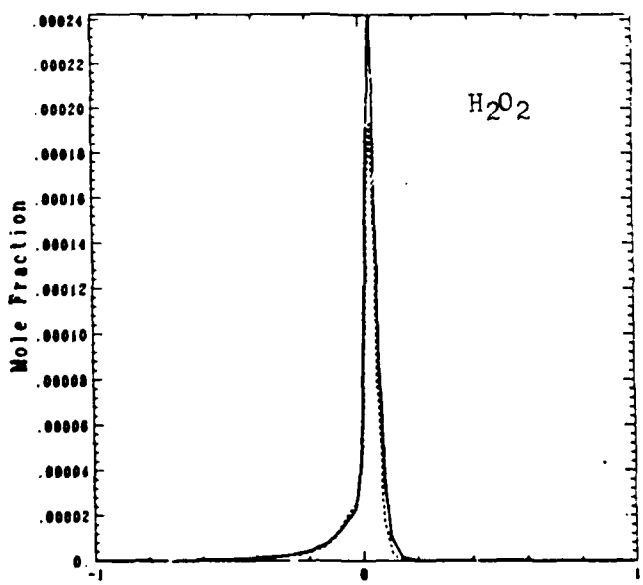

The rate constant was reduced still further to 300 1/s in Run 77 with the same temperature window. Again it is instructive to study the species profiles of this run displayed in Figure 29. The atomic oxygen maximum concentration is lower in this case than in the base case despite the inclusion of the photodissociation of O2. However, a prominent shoulder can be observed ahead of the flame, which begins at the location at which the mixture temperature exceeds the lower limit of the temperature window. As observed before in Run 67, the deposition of atomic oxygen ahead of the flame front can lower the thermally produced peak which follows. Due to the temperature window used in Run 67, the photodissociative deposition ceased before the thermal production commenced, producing a separated peak without enhancement. In Run 77, however, this deposition continues throughout the flame front giving a calculated flame speed of 55 cm/s, a 17% increase over the base case. The profiles for H and OH show similar behavior with lower peak values, but with both profiles displaced toward the unburnt gas. It may well be that these radicals are consumed in the more rapid destruction of the recombination products HO2 and H2O2, which here both exhibit considerably diminished peaks. The results of this run deserve further investigation. However, it is noteworthy that, at this level of oxygen dissociation slightly leading the flame front and continuing through it, the calculated flame speed is significantly enhanced.

3. Conclusions of the HCT Analytical Results

Based on these findings, we discuss more generally the role of radical deposition by photodissociation in combustion enhancement. The measure of enhancement which has been used is an increase in calculated flame speed. The objective of increasing flame speed is promoted by actions which cause the unburnt mixture to proceed more rapidly to products, here H2O. Increasing the pool of fast radicals (O, H, OH) via either photodissociation of O2 or HO2 should have this result. Recently, in related work performed at M.L. ENERGIA, Inc., under contract to the National Science Foundation, the beneficial effect of the photodissociation of HO2 on the second explosion limit in hydrogen/air mixtures has been investigated, both experimentally and analytically (9). It has been demonstrated that the photodissociation of the metastable HO2, which is the result of radical recombination (chain-terminating), is capable of extending the explosion limit. Similarily, the work discussed above has shown that photodissociation of HO2 as well as O2 results in a substantial increase in flame speed. Moreover, the runs considered here have shown that, in general, these two approaches of photodissociating O2 or HO2 act in concert. That is, an increase in concentration of fast radicals reduces HO2 concentration. Likewise, photodissociation of HO2 yields more O and OH. It remains to examine in more detail the effect of the precise characteristics of combined photodissociation of O2 and HO2 on enhancement.

FIGURE 29

SPECIES PROFILES FOR RUN 77 TABLE II
SOLID CURVES-BASE CASE, NO PHOTODISSOCIATION
DASHED CURVES-PHOTODISSOCIATION OF O2 WITH RATE CONSTANT 3E2 1/S
ABSCISSA IS RELATIVE FLAME POSITION (cm);
SPECIES INDICATED ON GRAPH

(a)

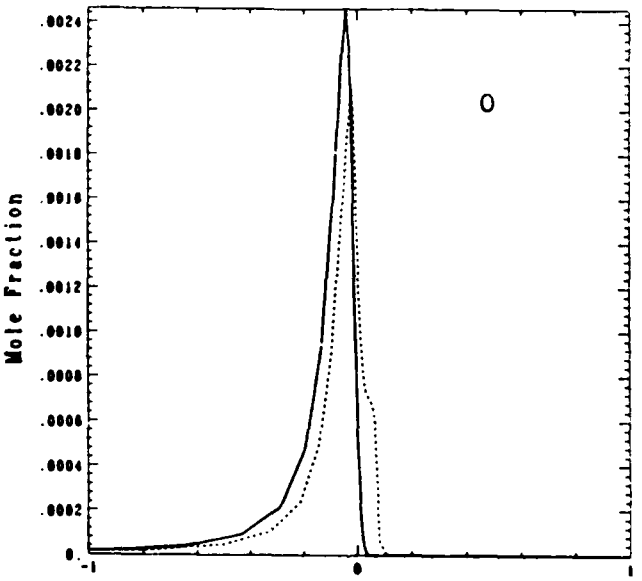

(b)

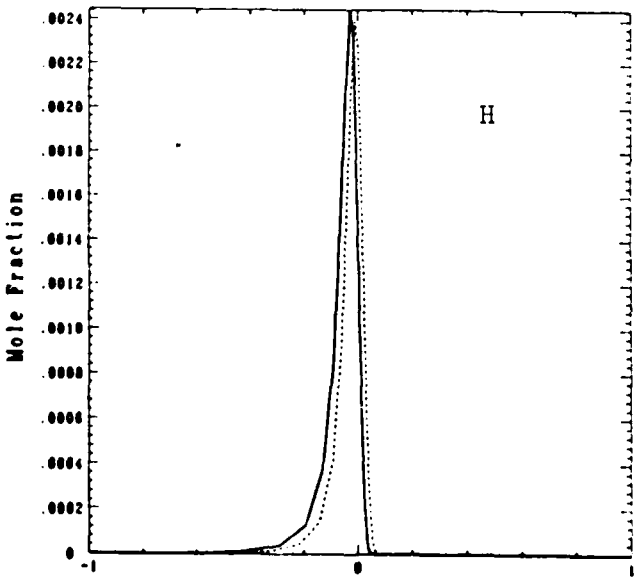

(c)

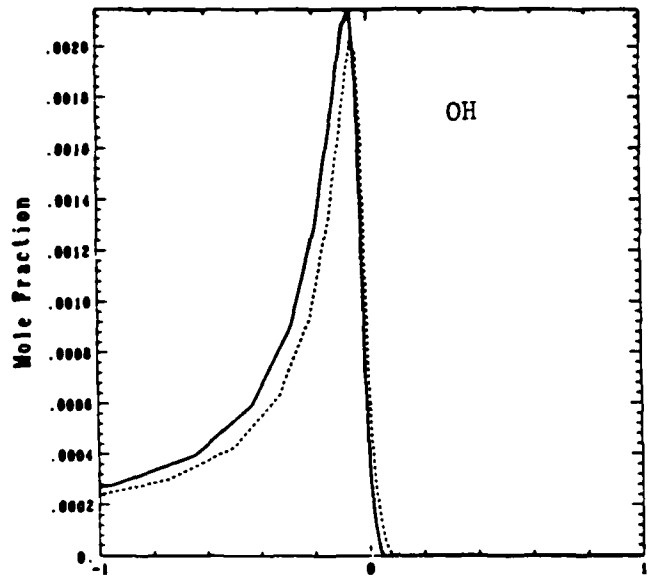

Figure 29

(continued)

(d)

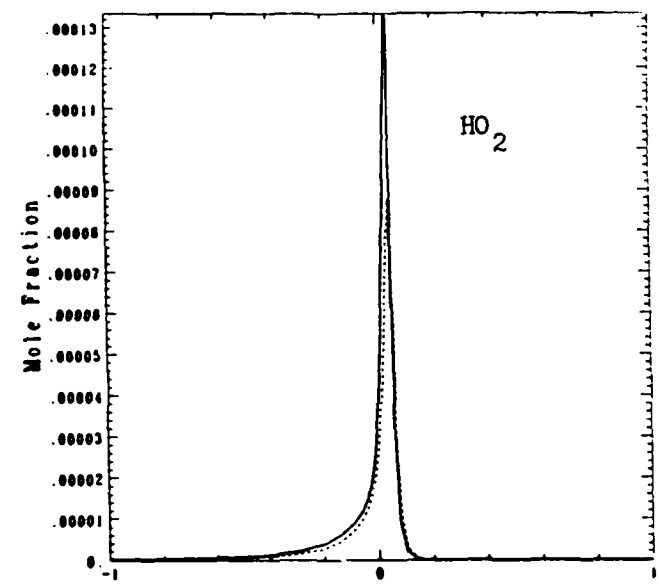

(e)

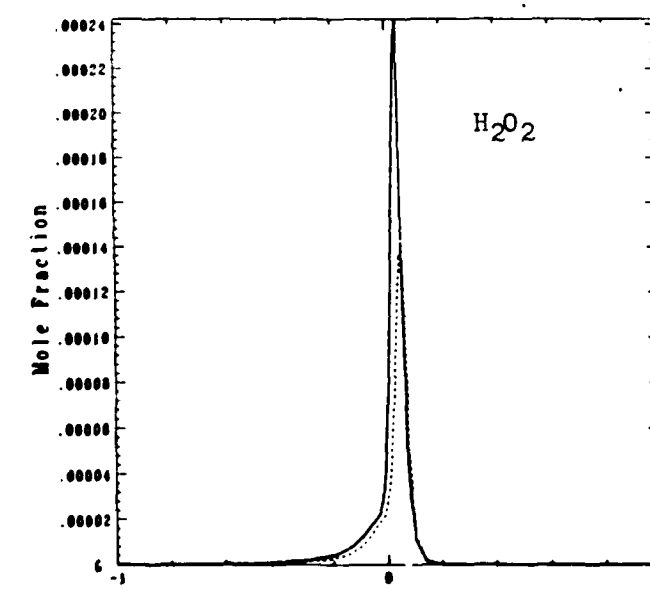

In considering the radical deposition achieved, there are three main factors: absorbing species, rate, and position. We have focussed on the photodissociation of O2 and HO2, the first giving two oxygen atoms and the second, an oxygen atom and a hydroxyl radical. With the rapid equilibration within the O-H-OH pool, there should be no clear advantage of the one over the other with respect to the product radicals. This expectation is confirmed when we examine the increase in flame speed obtained versus the rate of radical production for the two different absorbers (O2 and HO2). This rate is the product of the rate constant used times the absorber concentration. We compare Runs 76 (HO2) and 77 (O2) which gave nearly equal flame speeds (56-57 versus 55 cm/s). Let m be the total molar density (mol/cm3) of the mixture, which is nearly equal for the two cases at corresponding locations. The representative mole fraction of molecular oxygen at the flame front for Run 77 is taken to be 0.15, giving a concentration of 0.15 m. The rate of radical production in Run 77 is thus twice the rate of the dissociation of O2 or,

$$(2)(300)(0.15\ m) = 90\ m\ mol/cm3.s.$$

For Run 76, the representative mole fraction for HO2 used is 7E-5, approximately half the peak value of the base case profile with no HO2 dissociation. The resulting radical (O and OH) production rate is,

$$(2)(5E5)(7E\text{-}5\ m) = 70\ m\ mol/cm3.s.$$

The closeness of these two values suggests that the rate of radical deposition is more important than the species undergoing photodissociation.

The importance of the position of the radical deposition with respect to the flame front became apparent in the comparison of the results of Runs 69 (flame speed of 51 cm/s) and 72 (76 cm/s). As noted above, the only difference between these runs was that the temperature window used for Run 69 allowed the oxygen atom concentration to drop to the base case level before the thermal production commenced. In Run 72, the window (375-1300 K) was chosen to cause the two separate peaks to coalesce into a single broadened peak. Because the second window contains the first, it is true that more total energy was deposited in Run 72 than in Run 69. When the temperature and molecular oxygen profiles are superimposed, it is evident that the oxygen concentration is decreasing rapidly by the point the temperature has exceeded 700 K. Consequently, the difference in total absorbed energy would not be significant.

These observations also apply to the comparison of Runs 67 (flame speed of 47 cm/s) and 77 (55 cm/s), which again differs

only in the temperature window used, i.e., primarily in the position of radical deposition. The importance of optimizing this position appears to favor the photodissociation of HO2 in practical combustion systems. Becuase such systems generally operate fuel-lean, molecular oxygen would be present on both sides of the flame front, making it difficult to deposit the necessary short wavelength VUV energy (140-180 nm) at an optimal position in the flame front. In contrast, the HO2 peak is intrinsically in the correct position. In addition, the existence of wavelength regions in which HO2 (longer VUV wavelengths, 200-260 nm) is the primary absorber facilitates the delivery of the energy to this location. However, the low concentration of HO2 does require high intensity irradiation or efficient utilization of the incident photons (e.g., multiple pass optics) to achieve the desired rate of radical production.

With the use of the HCT model, we have thus been able to prove the fundamental chemistry of the propagating flame in the presence of the photodissociation of O2 and HO2 and thereby identify the key factors governing photochemical combustion enhancement. The effect of these factors on calculated flame speed and their inter-relationships have been explored in two series of runs, selected on the basis of extensive previous work. Basic insights gained from interpreting these results have provided valuable guidance for the experimental program and will continue to do so.

STATUS

In summary, during the last contract period the analytical effort has:

- o Developed a model for radiative ignition capable of analyzing the effects of flow on photochemical ignition.
- o Obtained analytical results which are in good conformity with our experimental data.
- o Clarified the role of Damkohler number, and demonstrated that our VUV lamp has sufficient output to achieve ignition even at low Damkohler numbers (supersonic flows).
- o Examined the effect of wavelength dependence on radiative ignition and concluded that short wavelengths ("hard" VUV) are most effective in photodissociating O2.
- o Corroborated experimental results that VUV radiative ignition favors fuel-lean mixtures over stoichiometric and fuel-rich mixtures.
- o Continued to use the HCT model to investigate radiative enhanced combustion and obtained analytical evidence for enhancement.

o Conducted two series of runs simulating both O2 and HO2 photodissociation, and concluded:

- Previously obtained double peak in O-atom concentration was an artifact of the temperature window used. It caused unwarranted depletion of radicals at the flame front, and thus preventing the flame from achieving its fullest potential velocity.

- Correcting this artifact resulted in dramatic increases in flame speed (62% and 29% for O2 and HO2 photodissociation, respectively).

o Identified three key factors governing radiative combustion enhancement; absorbing species, rate and position, and concluded:

- The rate of radical deposition is a more important factor than the species undergoing photodissociation (O2 or HO2).

- The position of deposition is also important, with the favored position being at or slightly ahead of the flame front.

PUBLICATIONS

1. Lavid, M., and Stevens, J.G., "Photochemical Ignition of Premixed Hydrogen/Oxidizer Mixtures with Excimer Laser", Combustion and Flame, 60, 2, (1985).

2. Lavid, M., Blair, D.W., and Stevens, J.G., "Photochemical Effect on the Second Explosion Limit of H2/O2 System; Experimental and Analytical Results".

3. Lavid, M., Stevens, J.G., and Westbrook, C.K., "Enhancement of Premixed H2/Air Flames with Photochemically Produced Radicals-Analytical Modeling".

4. Lavid, M., and Blair, D.W., "Experimental and Analytical Results of Radiative Ignition in Premixed Hydrogen-Air Flows".

Papers 2 thru 4 are in preparation for submission to either Twenty-First International Symposium on Combustion, Combustion and Flame or Combustion Science and Technology. Similar topics will be submitted for presentation at the 1985 Technical Meeting of the Eastern Section of Combustion Institute in Philadelphia, Pennsylvania.

PROFESSIONAL PERSONNEL
ASSOCIATED WITH RESEARCH EFFORT

Dr. Moshe Lavid - Principal Investigator - PhD Mechanical Engineering, State University of New York at Stony Brook, 1974.

Dr. David W. Blair - Senior Staff Member - PhD Mechanical Engineering, Columbia University, 1961.

Dr. Arthur T. Poulos - Research Staff Member - PhD Physical Chemistry, Northwestern University, 1976.

Dr. J. G. Stevens - Analytical Consultant - PhD Courant Institute of Mathematic Sciences, New York University, 1972.

Dr. Charles K. Westbrook - Analytical Consultant - PhD Engineering/Applied Science, University of California at Davis, 1974.

INTERACTIONS

A. Presentations

Four presentations on Radiative Augmented Combustion were made during this reporting period as follows:

- o Drexel University MEM Department, Philadelphia, Pennsylvania.
- o AFOSR Contractors Meeting, Pittsburgh, Pennsylvania.
- o Department of Mechanical Engineering, Technion, Haifa, Israel.
- o 1984 Technical Meeting of the Eastern Section of the Combustion Institute, Clearwater Beach, Florida.

B. Interest Expressed by Other Researchers

The interest in the whole subject of combustion enhancement is continually expanding. Ward and Wu (10) proposed microwave radiation as a means of enhancing the flame speed to allow use of lean mixtures in spark-ignition engines. According to their theory, the microwave field principally heats the electrons of the flame, and the hot electrons transfer energy to the reacting species. The resulting increase in the population of higher vibrational states of the reacting species, especially that of oxygen, is said to increase reaction rates in the flame, as suggested by Jaggers and von Engel (11). This increase in the reaction rates is expected to be greater than that which results from simple thermal heating of the bulk gases. Ward (12,13) compared theoretically and experimentally cavity quality factors and concluded that the microwave flame-plasma interaciton was strong as predicted. Additional work by Ward (14) in a constant-volume combustion bomb suggests that burn time can be reduced by the application of microwaves in conjunction with plasma-jet ignition. Subsequent experiments by Clements and coworkers (15,16) show that the flame-plasma electrons are heated and that changes in flame speed are on the order of 5% to 10% when gas breakdown does not occur.

Recently, several researcher (17) at General Motors Research Laboratory reported an increase of 6% in burning velocity of fuel-lean premixed laminar flames with microwave radiation. However, they concluded that the enhancement is not due to a radiative (photochemical) effect but rather due to a thermal effect. The increase in flame speed is explained in terms of simple microwave heating of the bulk gases in the flame zone, which yields a higher flame temperature. ENERGIA has established open commumication with Drs. T. Sloane, R. Hickling and E. Groff from the General Motors group.

Interest in our Radiative Augmented Combustion is reflected by the many requests for additional technical information listed below. Special interest was expressed by researchers working on plasma jet ignition and flameholding such as Professor Felix Weinberg at Imperial College, London, Professor Eli Dabora at the University of Connecticut and Dr. G. Burton Northam at NASA Langley, Hampton, Virginia. NASA's interest in our radiative technique has been pursued to a cooperative experiment in which ENERGIA provides the VUV light sources to be mounted on NASA supersonic combustion facility. The objective is to determine the feasibility of utilizing VUV photodissociation for ignition and flameholding in supersonic flows (scramjets), which are known to be very difficult to ignite. A very limited and preliminary test was already conducted on NASA's Mach 2 combustor. The results and conclusions are given in the section Experimental Effort. This collaboration is planned to be continued.

Another strong interest in our research was expressed by Dr. Lyle O. Hoppie of the Eaton Corporation. They investigate another approach for achieving enhanced combustion. They preheat the fuel to about 550 C prior to injection. Recent reported results (18) are that reduction in ignition delay time and increase in combustion rate are obtained.

In a related work under a grant from the National Science Foundation, the concept of Radiative Augmented Combustion was successfully demonstrated (9). The idea was to promote combustion through photodissociation of reaction-inhibiting species into reactive radicals which participate in chain-branching reactions. This idea was tested in H2/air system by investigating its capability to extend the second explosion limit. It is well known that this limit is attributed to three body reaction, H + O2 + M ---> HO2 + M, followed by the removal of HO2 from the kinetic scheme. This reaction becomes increasingly important at higher pressures where it competes fiercely with the chain-branching reaction, H + O2 ---> OH + O.

This research demonstrated that the photodissociation of the metastable radical HO2, HO2 + hv ---> OH + O, can effectively compete with the terminating reactions. It restores radicals to the pool and mitigates the influence of the three body reaction. The experimental evidence for this was an affirmative extension of the second explosion limit. Increases in the pressure limit as great as 24% percent were obtained.

During this period the following professionals expressed interest in our research:

Dr. Steven L. Baughcum, Los Alamos Natinal Laboratory, New Mexico.

Mr. Theodore A. Brabbs, NASA Lewis Cleveland, Ohio.

Dr. Claudio Bruno, Dipartimento di Energetica, Politecnico di Milano, Italy.

Dr. Hartwell F. Calcote, Aero Chem Research Lab., Princeton, New Jersey.

Prof. Eli K. Dabora, University of Connecticut, Storrs, Connecticut.

Prof. Peter Gray, University of Leeds, England.

Dr. Edward G. Groff, GM Research Laboratories, Warren, Michigan.

Dr. Alan Hartford, Los Alamos Scientific Lab, New Mexico.

Prof. Clarke E. Hermance, University of Vermont, Burlington, Vermont

Dr. Lyle O. Hoppie, Eaton Corportation, Southfield, Michigan.

Dr. David Mann, US Army Research Office, Research Triangle Park, North Carolina.

Prof. Arthur M. Mellor, Drexel University, Philadelphia, Pennsylvania.

Dr. G. Burton Northam, NASA, Langley Research Center, Hampton, Virginia.

Prof. Herschel Rabitz, Princeton University, Princeton, New Jersey.

Dr. Ramohalli, Flow Industries, Inc. Kent, Washington.

Dr. Felix Schuda, ILC Technology, Sunnyvale, California.

Prof. K. Seshadri, University of California, La Jolla, California.

Dr. Tom Sloane, GM Research Laboratories, Warren, Michigan.

Prof. Felix Weinberg, Imperial college, London, England

Dr. Charles K. Westbrook, Lawrence Livermore Laboratory, University of California, Livermore, California.

SUMMARY: ASSESSMENT OF RESEARCH RESULTS

This research has demonstrated the capability of the radiative technique to both ignite and enhance combustion processes and to broaden normally encountered stability limits.

The research on radiative ignition and combustion enhancement is providing fundamental information on a unique combustion process. Concepts which represent a new departure and extension of conventional combustion practice can evolve from the experimental and analytical results being obtained. Aspects of the radiative ignition and enhancement concept have been already demonstrated under both static and flow conditions. Successful pulsed light source ignition experiments at very high flow velocities (up to 250 m/s) reconfirm the radiative augmented concept and demonstrate the technical feasibility of designing an advanced optical-radiative igniter. Potential radiative ignitions with a continuous light source imply the possibility of using the light as an optical radiative flame stabilizer with no pressure loss instead of the conventional intrusive flameholders. Preliminary experimental results of radiative combustion enhancement in terms of higher flame speeds and larger extinction times and distances suggest an opportunity to extend the combustor operating limits. It is based on knowledge that the increase in flame speed is indicative of higher combustion rate which can result in extension of the operating envelope of flashback and blow-off limits.

The extensive analytical results reported here, in particular, the dramatic increases of up to 62% in flame speed, give us confidence that radiative augmented combustion can become a potentially viable technique for extending current aircraft operating limits associated with combustion phenomena. However, more supportive experimental results are needed before eventual application to gas turbine engine systems can be envisioned both for improved combustor operation and flameholding. Some future areas of potential application are: high altitude combustor reignition following flame-out, drag-free flame stabilization in supersonic combustor, and added flexibility for conventional combustors to use future alternate fuels. To this end, additional radiative ignition and combustion enhancement experiments under flow condiitons are planned to be conducted during the third year of this program, together with a continued VUV light source development in the direction of improved beam intensity and optics.

REFERENCES

1. Technical Proposal For Radiative Augmented Combustion, M.L. ENERGIA, Inc., ENG No. 101, 1982.
2. Technical Proposal for Radiative Augmented Combustion, M.L. ENERGIA, Inc., ENG No. 102 Revised, 1984.
3. Lavid, M., "Radiative Augmented Combustion", First Annual Technical Report AFOSR-TR-84- , Contract No. F49620-83-C-0133, also M.L. ENERGIA, Inc. Report No. ENG 101 ATR 8408, August 1984.
4. Lavid, M. and Stevens, J.G., "Photochemical Ignition of Premixed Hydrogen/Oxidizer Mixtures with Excimer Laser", Combustion and Flame 60, 2, :195-202 (1985).
5. Technical Proposal for Radiative Augmented Combustion, M.L. ENERGIA, Inc., ENG No. 103, 1985.
6. Northam, G.B., and McClinton, C.R., "Development and Evaluation of a Plasma Jet Flameholder for Scramjets", 20th Joint Propolsion Conference, A1AA-84-1408, 1984.
7. Cerkanowicz, A.E. and Bartok, W., "Radiation Augmented Combustion", Interin Technical Report AFOSR-TR-78-1508, July 1978.
8. Lavid, M., Stevens, J.G., and Westbrook, C.K., "Analytical Modeling of Radiative Enhancement in Premixed Hydrogen-Air Flames", Technical Meeting of Eastern Section: Combustion Institute, Clearwater Beach, Fl., 1984.
9. Lavid, M., Blair, D.W., and Stevens, J.S., "Modifying Combustion Kinetics by Photodissociation of Inhibitors", Final Report, NSF Grant No. CPE-8460827, 1985.
10. Ward, M.A.V., and Wu, T.T., Combus. Flame 32: 57-71 (1978).
11. Jaggers, H.C., and von Engel, A., Combus. Flame 16: 275-285 (1971).
12. Ward, M.A.V., J. of Microwave Power 12(3): 187-199 (1977).
13. Ward, M.A.V., J. of Microwave Power 14(3): 241-259 (1979).
14. Ward, M.A.V., J. of Microwave Power 15(3): 193-202 (1980).
15. Clements, R.M., Smith, R.D., and Smy, P.R., Comb. Sci, and Tech. 26: 77-81 (1981).
16. MacLatchy, C.S., Clements, R.M., and Smy; P.R., Combus. Flame 45: 161-169 (1982).
17. Groff, E.G. and Krage, M.K., Combustion and Flame 56, 293-306 (1984).
18. Scharnweber, D.H., and Hoppie, L.O., "Hypergolic Combustion in an Internal Combustion Engine", SAE 850089, 1985.

APPENDIX A

A Model for Radiative Ignition in Flow Systems

Radiative ignitions of flammable gas mixtures have been repeatedly demonstrated in static systems (1-5), and more recently also in flowing systems. It has become necessary to supplement the experimental effort with a theoretical investigation of the effects of flow on radiative ignition.

In a typical radiative ignition experiment, ignition is obtained through the absorption of ultraviolet radiation from a pulsed short arc lamp. The radiation pulse widths are of the order of 1E-4 s. In a static system a given fluid element is exposed to the radiation during the entire period of the pulse, and if sufficient photons are absorbed during the pulse to produce radicals in excess of a critical concentration, ignition occurs. Theoretical calculations, which have been presented in previous reports (3), have determined the critical radical concentrations that are required to produce ignition.

In a flowing system the situation is changed in that a given fluid element moves relative to the radiation field during the pulse, and it sees a different intensity-time relationship than would be the case in a static system. If the time of passage of a fluid element through the radiation field is very long relative to the pulse width, then the system is quasi-static, but if the time of passage is short relative to the pulse width the system is truly dynamic. It is the Damkohler number (D) that differentiates between static and dynamic ststems. It is defined as the ratio of the convective time across the radiation field to the radiation pulse width. For D's greater than unity the system is considered static, and for D's equal or less than unity it is a dynamic system.

The analysis of this section addresses the criticality ratio which is the ratio of the radical concentration that is produced photochemically in a dynamic system relative to the critical concentration required for ignition (which should be the same for static or dynamic systems). If this critical concentration is exceeded, ignition is said to occur. This calculation can also be used as the initiation input to a kinetic calculation which will then follow the development of the combustion reactions. In this work however, it is restricted to calculating the radical concentration achieved relative to the critical value, i.e. determining the criticality ratio.

The Model

The model is based upon the continuity equation with ignition being initiated by a pulse of ultraviolet radiation. It is assumed that each active photon produces ki radicals of species, Ri, i.e. it considers the reaction,

$$A + h\nu \longrightarrow k_i R_i$$

The continuity equation may be written as,

$$1.) \quad \frac{\partial Y_i}{\partial t} + \bar{V} \cdot \nabla Y_i = \frac{w_i}{\rho} - \frac{[\nabla \cdot (\rho Y_i \bar{V}_i)]}{\rho}$$

where:

$Y_i \equiv$ mass fraction of species i

$t \equiv$ time, s

$V \equiv$ mass average velocity, cm/s

$\rho \equiv$ mass density, g/cm3

$w_i \equiv$ mass rate of production species i, g/cm3 s

$\bar{V}_i \equiv$ diffusion velocity of species i relative to mass average velocity, cm/s

The species production rate is taken as the sum of a photochemical rate and a non-photochemical rate:

$$w_i = w_{ip} + w_{ich}$$

where:

$w_{ip} \equiv$ mass rate of production of species i through induced photochemical reactions

$w_{ich} \equiv$ mass rate of production of species i by all other chemical reactions

In terms of number densities the chemical terms can be written as,

$$w_i = \frac{M_i}{N_A} \dot{n}_i$$

and for the photochemical reaction in particular,

$$\dot{w}_{ip} = \frac{M_i}{N_A} \dot{n}_{ip}$$

where:

$M_i \equiv$ molecular weight of species i, g/mole

$N_A \equiv$ Avogadro's number, molecules/gmole

$\dot{n}_{ip} \equiv$ number rate of production of species i through induced photochemical reactions, 1/cm3 s

For the photochemical reaction,

$$A + h\nu \rightarrow k_i R_i$$

$$\dot{n}_{ip} = -k_i \nabla \cdot \bar{\dot{m}}_p$$

where:

$\bar{\dot{m}}_p \equiv$ the photon flux rate vector, photons/cm2 s

In the case of photons of a single frequency and propagating along a path ℓ,

where:

$$d\bar{\ell} = \hat{i}\,dx + \hat{j}\,dy + \hat{k}\,dz$$

$$\nabla \cdot \bar{\dot{m}}_p = -\alpha_p \dot{m}_{po} \exp\left[-\alpha_p(\ell - \ell_o)\right]$$

and,

$$\dot{n}_{ip} = k_i \alpha_p \dot{m}_{po} \exp\left[-\alpha_p(\ell - \ell_o)\right]$$

where:

$\alpha_p \equiv$ optical absorption coefficient, 1/cm

$\dot{m}_{po} \equiv$ input photon flux at $\ell = \ell_o$ photons/cm2 s

$\ell \equiv$ distance along optical path, cm

In these terms, the rate of production of species i becomes:

$$\omega_i = \frac{M_i}{N_A} k_i \alpha_p \dot{m}_{po} \exp\left[-\alpha_p (l - l_o)\right] + \omega_{ich}$$

and equation (1) becomes:

$$2.) \quad \frac{\partial Y_i}{\partial t} + \bar{V} \cdot \nabla Y_i = \frac{M_i k_i \alpha_p \dot{m}_{po} \exp\left[-\alpha_p (l - l_o)\right]}{N_A \rho} + \frac{\omega_{ich}}{\rho} - \frac{\left[\nabla (\rho Y_i \bar{V}_i)\right]}{\rho}$$

The equation is now put into dimensionless form by defining the dimensionless time $\tilde{\tau}$ and distance θ as:

$$\tilde{\tau} \equiv \frac{t}{t_i}$$

$$\theta \equiv \frac{l}{L}$$

where: ti is the photo-pulse width and L is a characteristic lateral dimension of the input light beam.
If the velocities are written as;

$$\bar{V} = \nu \hat{V}$$

$$\bar{V}_i = \nu_i \hat{V}_i$$

where: v; vi are scaler magnitudes, $\hat{V}$ and $\hat{V}_i$ are unit vectors, and Yi is expressed relative to its critical value through:

$$F \equiv \frac{Y_i}{Y_{ic}}$$

where: Yic is the critical mass ratio of i required to produce ignition.

Equation (2) can be written as:

$$3.) \quad \frac{\partial F}{\partial \tau} + \frac{1}{D_1} \hat{V} \cdot \nabla F = \frac{t_i}{t_c} + \frac{t_i \omega_{ich}}{Y_{ic} \rho} - \frac{t_i N_i}{L} \nabla \cdot (F \hat{V}_i)$$

In eq. (3), ∇ is now taken in terms of $\theta \cdot D_1$, Damkohler's first number, is defined as the ratio of convective time to chemical time. It is expressed in a dimensionless form as:

$$D_1 \equiv \frac{L}{N t_i}$$

The critical time, t_c, is defined as:

$$4a.) \quad t_c \equiv \frac{N_A \rho Y_{ic}}{M_i k_i \alpha_p \dot{m}_{po} \exp[-\alpha_p (l - l_o)]}$$

Or, noting that,

$$Y_{ic} = \frac{n_{ic} M_i}{N_A \rho}$$

$$4b.) \quad t_c = \frac{n_{ic}}{k_i \alpha_p \dot{m}_{po} \exp[-\alpha_p (l - l_o)]}$$

where:

tc is the time it takes an element of gas at depth $l - l_0$ to achieve critical radical mass ratio Y_{ic} as a result of photon input $\dot{m}_{po}$ in the absence of all other effects. The ratio ti/tc is the ratio of radiation input pulse width to this critical time.

Equation (3) is the general working equation for the case of input photon flux $\dot{m}_{po}$ representing photons of a single wavelength. A real radiation source has a finite spectral bandwidth, and its input is specified in terms of an intensity I. The overall intensity, I_o, is specified as watts/cm2 steradian while the spectral intensity, I_λ, of which it is composed is specified in terms of watts/cm2 steradian nm, where wavelength λ is expressed in terms of nanometers.

The term in eq. (3) that is affected by this change is the first term on the right hand side, ti/tc.

The spectral distribution of pulsed light source that is used in this work (the ILC source) was measured by Cerkanowicz (7). It was reported as I_R versus λ in the spectral region from 142.5 to 250 nm. The relative intensity I_R is defined in terms of a standard intensity I_{std} (i.e. $I_R \equiv I_\lambda / I_{std}$). Assuming that I_R is independent of I_{std} one can write for any intensity Io,

$$I_o = I_{std} \int_{\lambda_1}^{\lambda_2} I_R \, d\lambda$$

Combining this with the definition of I_R results in:

$$I_\lambda = \frac{I_o \, I_R}{\int_{\lambda_1}^{\lambda_2} I_R \, d\lambda}$$

The energy at wavelength λ absorbed at a point at depth $\ell - \ell_o$ in the gas is given by,

$$I_\lambda \alpha_\lambda \exp\left[-\alpha_\lambda (\ell - \ell_o)\right] d\lambda$$

The photon flux contained in I_λ is:

$$\dot{m}_\lambda = \frac{I_\lambda \lambda}{hc}$$

where:

h $\equiv$ Planck's constant

C $\equiv$ velocity of light in vacuum

The rate of photon absorption at an interior point in the gas as a result of input radiative intensity Io at its surface (assume a parallel input and surpress the units of steradians) is:

$$\frac{I_o}{hc \int_{\lambda_1}^{\lambda_2} I_R d\lambda} \int_{\lambda_1}^{\lambda_2} \alpha_\lambda \lambda I_R \exp\left[-\alpha_\lambda (\ell - \ell_o)\right] d\lambda$$

The term t_i/t_c in eq. 3 now becomes:

5.) $$\frac{M_i \cdot k_i \cdot t_i}{N_A \rho Y_{ic}} \frac{I_o}{hc \int_{\lambda_1}^{\lambda_2} I_R d\lambda} \int_{\lambda_1}^{\lambda_2} \alpha_\lambda \lambda I_R \exp\left[-\alpha_\lambda (\ell - \ell_o)\right] d\lambda$$

or alternatively,

$$\frac{k_i I_o t_i}{n_{ic} hc \int_{\lambda_1}^{\lambda_2} I_R \, d\lambda} \int_{\lambda_1}^{\lambda_2} \alpha_\lambda \lambda I_R \exp\left[-\alpha_\lambda (\ell - \ell_o)\right]$$

In these terms, for the spectrally distributed case, equation (3) becomes:

6.) $$\frac{\partial F}{\partial \tau} + \frac{1}{D_1} \hat{V} \cdot \nabla F =$$

$$\frac{t_i k_i I_o}{n_{ic} hc \int_{\lambda_1}^{\lambda_2} I_R \, d\lambda} \int_{\lambda_1}^{\lambda_2} \alpha_\lambda \lambda I_R \exp\left[-\alpha_\lambda (\ell - \ell_o)\right] d\lambda$$

$$+ \frac{t_i \nu_{ich}}{Y_{ic} \rho}$$

$$- \frac{t_i \nu_i}{L} \nabla \cdot (F \hat{V}_i)$$

This result was used to model the two-dimensional case in which flow is along the positive x-axis and radiative input is along the positive y-axis as is shown in figure 1A.

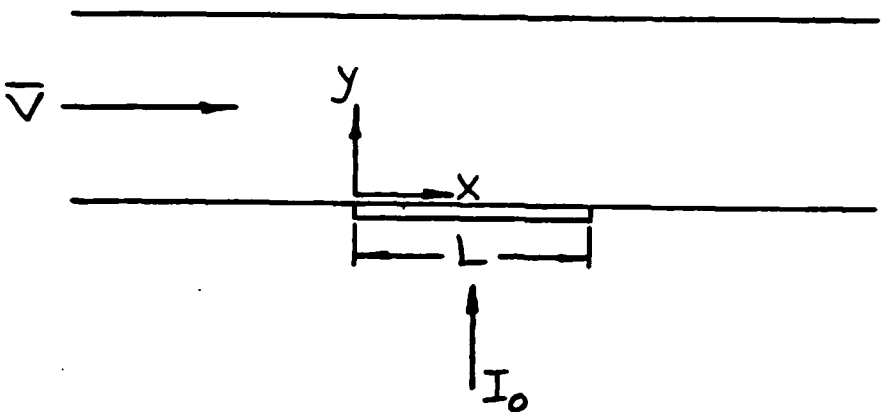

Figure 1A
Schematic Diagram of the Two-dimensional Problem

The input radiation Io is a parallel beam, diffusion velocity, vi, is taken as negligible, and the chemical reaction rate which is also taken as negligible. Ignoring vi (a good assumption on the time scale of the radiative pulse) effectively decouples the space dimensions x and y (this coupling is achieved solely through the radiative input), and renders the problem quasi-one dimensional.

The resulting equation is:

$$7.) \quad \frac{\partial F}{\partial Z} + \frac{1}{D_1} \frac{\partial F}{\partial X} = A(Z)$$

where:

$$A(Z) = \frac{t_i \, k_i \, I_o}{n_{ic} \, hc \int_{\lambda_1}^{\lambda_2} I_R \, d\lambda} \int_{\lambda_1}^{\lambda_2} \alpha_\lambda \lambda I_R \exp\left[-\alpha_\lambda L Z\right] d\lambda$$

The dimensionless space coordinates along the x and y directions are designated as X and Z, respectively.

The equation is solved for the conditions:

$$\bar{V} = \text{constant}$$

$F = 0$ for $\tau = 0$ for all X, Z

$F = 0$ for $X = 0$ for all τ, Z

It is put into backward difference form and solved numerically:

$$8.) \quad F_{i,j,k} = \frac{A(Z_i) + \frac{F_{i,j,k-1}}{\Delta Z} + \frac{F_{i-1,j,k}}{D_1 \Delta X}}{\frac{1}{\Delta Z} + \frac{1}{D_1 \Delta X}}$$

The indices i, j, k refere to X, Z, τ, respectively.

The relative lamp intensity, I_R, was scaled from Figure 10, while the spectral absorption coefficient, α_λ, was taken as that for O2 from Figure 11 in the text. They were used to form Table IA which was used as input data.

In computing A(Z) it was assumed that α_λ was constant throughout space. This is a good assumption when F is small, because then the density of molecular oxygen is essentially constant throughout space. However, for high levels of dissociation (F > 100) this is a poor assumption (dissociation is approximately 6 percent at F=100) and for F > 800 it is an unsupportable assumption. Future work will omit the assumption of constant α_λ and allow it to vary throughout the field.

Table IA

Spectral Data Used In Computation

LAMBDA,nm	Irelative	ALPHA,1/cm
142.5	.2	396
145	.57	375
147.5	.75	337
150	.78	290
152.5	.41	250
155	.39	200
157.5	.34	159
160	.35	122
162.5	.26	85
165	.3	55
167.5	.33	33
170	.32	20.4
172.5	.29	12.6
175	.27	3
177.5	.17	.43
180	.14	.113
182.5	.1	.039
185	.065	.0113
187.5	.07	.0052
190	.055	.00202
192.5	.065	.00104
195	.05	.00053
197.5	.045	.000425
200	.055	.000349
202.5	.06	.000325
205	.06	.000303
207.5	.08	.000278
210	.1	.000254
212.5	.105	.000235
215	.13	.000206
217.5	.15	.000183
220	.18	.000161
222.5	.19	.000139
225	.17	.000119
227.5	.24	.0001
230	.28	8.41E-5
232.5	.29	6.33E-5
235	.26	4.95E-5
237.5	.23	3.89E-5
240	.21	2.87E-5
242.5	.24	1.97E-5
245	.25	1.35E-5

Inclusion of O Atoms Recombination

The effect of oxygen atom recombination is added to the model, and is included in the chemical reaction term ω_{ich} defined above.

The three body oxygen atom recombination reaction is:

$$O + O + M \xrightarrow{k_o} O_2 + M$$

$$\frac{d[O]}{dt} = -2k_o[O]^2[M] \quad \text{moles/cm}^3\text{sec}$$

$$\omega_{ich} = M_i \frac{d[O]}{dt}$$

where subscript i refers to the O-atom.

The density of the overall mixture changes even at constant T, P as the total number of moles changes.

The starting mixture is, $A H_2 + B O_2$

$$N_H = 2A$$

$$N_O = 2B$$

$$\frac{d[O]}{dt} = -2k_o[O]^2[M]$$

which is the same as,

$$\frac{d\rho_o}{dt} = -2k_o \rho_o^2 \rho_M$$

where: $\rho_o = \frac{n_o}{N_A}$, moles/cm3

$n_o \equiv$ oxygen atom number density

$$Y_{ic} = \frac{n_{ic}}{N_A} M_i / \rho_{mass} \equiv Y_{oc}$$

$$Y_i = \frac{n_i}{N_A} M_i / \rho_{mass} \equiv Y_o$$

where: ρ, the mixture mass density, is explicitely indicated as moles/cm3 mass.

$$F = \frac{Y_i}{Y_{ic}} = \frac{n_i}{n_{ic}}$$

$$\rho_i = \frac{n_{ic} F}{N_A} \qquad moles/cm^3$$

$$\frac{d\left[\frac{n_{ic} F}{N_A}\right]}{dt} = -2 k_o \left[\frac{n_{ic} F}{N_A}\right]^2 \rho_M$$

$$w_{ich} = M_i \frac{d\rho_i}{dt}$$

$$w_{ich} = -2 k_o M_o \left[\frac{n_{oc} F}{N_A}\right]^2 \rho_M$$

This expression for w_{ich} contains two variables, F and ρ_M.

The third bodies are O2 and H2,

$$\rho_M = \rho_{H_2} + \rho_{O_2} \quad \text{moles/cm3}$$

The number of moles of O2 is given by:

$$N_{O_2} = N_{O_{2_I}} - \frac{1}{2} N_O$$

$$\rho_{O_2} = \rho_{O_{2_I}} - \frac{1}{2} \rho_O$$

But,

$$\rho_O = \rho_{Oc} F$$

$$\rho_{O_2} = \rho_{O_{2_I}} - \frac{1}{2} \rho_{Oc} F$$

$$\rho_M = \rho_{H_2} + \rho_{O_{2_I}} - \frac{1}{2} \rho_{Oc} F$$

$$\rho_M = \rho_I - \frac{1}{2} \rho_{Oc} F$$

Where: ρ_I the initial molar density of the mixture,

$$\rho_I = \frac{P}{RT}$$

$$w_{ich} = -2 k_0 M_i \left[\frac{n_{oc} F}{N_A}\right]^2 \left[\rho_I - \frac{1}{2}\rho_{oc} F\right]$$

$$= -2 k_0 M_i \left[\frac{n_{oc}}{N_A}\right]^2 \left[\rho_I F^2 - \frac{1}{2}\rho_{oc} F^3\right]$$

The second term on the right of eq. (3) becomes:

$$\frac{t_i w_{ich}}{\rho_{mass} Y_{ic}} = \frac{-2 t_i k_0 M_i \left[\frac{n_{ic}}{N_A}\right]^2 \left[\rho_I F^2 - \frac{1}{2}\rho_{ic} F^3\right]}{\rho_{mass} Y_{ic}}$$

Now,

$$\rho_{mass} = \rho_I M_w = \frac{P}{RT} M_w$$

Where M_w is the molecular weight of the mixture,

$$M_w = \frac{2 N_{H_2} + 32 N_{O_2} + 16 N_O}{N_{H_2} + N_{O_2} + N_O}$$

$$= \frac{2 \rho_{H_2} + 32 \rho_{O_2} + 16 \rho_O}{\rho_{H_2} + \rho_{O_2} + \rho_O}$$

$$= \frac{2\rho_{H_2} + 32\left(\rho_{O_{2_I}} - \frac{1}{2}\rho_{oc}F\right) + 16\rho_{oc}F}{\rho_{H_2} + \rho_{O_{2_I}} - \frac{1}{2}\rho_{oc}F + \rho_{oc}F}$$

$$= \frac{2\rho_{H_2} + 32\rho_{O_{2_I}}}{\rho_{H_2} + \rho_{O_{2_I}} + \rho_{oc}F}$$

$$\rho_{mass} = \rho_I \left[\frac{2\rho_{H_2} + 32\rho_{O_{2_I}}}{\rho_{H_2} + \rho_{O_{2_I}} + \rho_{oc}F}\right]$$

$$= \rho_I \left[M_{W_I}\right] \left[\frac{\rho_{H_2} + \rho_{O_{2_I}}}{\rho_{H_2} + \rho_{O_{2_I}} + \rho_{oc}F}\right]$$

$$= \rho_{mass_I} \left[\frac{\rho_{H_2} + \rho_{O_{2_I}}}{\rho_{H_2} + \rho_{O_{2_I}} + \rho_{oc}F}\right]$$

Where subscript I refers to initial conditions,

$$\frac{t_i w_{ich}}{\rho_{mass} Y_{ic}} = -\frac{2 t_i k_o M_i \left[\frac{n_{ic}}{N_A}\right]^2}{\rho_{mass_I} Y_{ic}} \frac{\left[\rho_I F^2 - \frac{1}{2}\rho_{oc}F^3\right]}{\left[\frac{\rho_{H_2} + \rho_{O_{2_I}}}{\rho_{H_2} + \rho_{O_{2_I}} + \rho_{oc}F}\right]}$$

$$9.) \quad \frac{t_i \dot{w}_{ich}}{\rho_{mass} Y_{ic}} = -\frac{t_i}{t_{ch}} \frac{\left[\frac{\rho_I}{\rho_{oc}} F^2 - \frac{1}{2} F^3\right]}{\left[\frac{\rho_{H_2} + \rho_{O_2 I}}{\rho_{H_2} + \rho_{O_2 I} + \rho_{oc} F}\right]}$$

Where t_{ch} in the dimensionless group $\frac{t_i}{t_{ch}}$ is given by:

$$\frac{1}{t_{ch}} \equiv \frac{2 k_o M_i \left[\frac{n_{ic}}{N_A}\right]^2 \rho_{oc}}{\rho_{mass_I} Y_{ic}}$$

$$= \frac{2 k_o M_i \rho_{oc}^3}{\rho_{mass_I} Y_{ic}}$$

$$= \frac{2 k_o M_i \rho_{ic}^3}{\rho_{mass_I} Y_{ic}}$$

Eq. (9) is the expression for the next to the last term in eq (6). Thus, it must be added to the right hand side of eq. (7) in order to account for oxygen atoms recombination. Similarly, in eq. (8) it adds directly to the term A(Z).

END

FILMED

5-86

DTIC